www.itcon.org - Journal of Information Technology in Construction - ISSN 1874-4753

3D GAUSSIAN SPLATTING IN CONSTRUCTION – FUNDAMENTALS AND APPLICATIONS

SUBMITTED: July 2026
PUBLISHED: November 2026
EDITOR: Rober Amor
DOI: 10.36680/j.itcon.2026.060

Niels Bartels
TH Köln, 50679 Cologne, Germany
https://orcid.org/0000-0001-7517-3422
niels.bartels@th-koeln.de

Urs Riedlinger
Fraunhofer FIT, 53757 Sankt Augustin, Germany
https://orcid.org/0000-0002-7406-5486
urs.riedlinger@fit.fraunhofer.de

Georgios Toubekis
Fraunhofer FIT, 53757 Sankt Augustin, Germany
https://orcid.org/0000-0002-9565-4917
georgios.toubekis@fit.fraunhofer.de

Philipp Hagedorn
Ruhr University Bochum, 44801 Bochum, Germany
https://orcid.org/0000-0002-6249-243X
philipp.hagedorn-n6v@rub.de

Patrick Herbers
Ruhr University Bochum, 44801 Bochum, Germany
https://orcid.org/0000-0002-9498-552X
patrick.herbers@rub.de

Fabio Pinto da Silva
Universidade Federal do Rio Grande do Sul (UFRGS), Porto Alegre - RS, CEP 90040-020, Brazil
https://orcid.org/0000-0001-9349-5601
fabio.silva@ufrgs.br

Carlos Berta Dohrn
Universidade Federal do Rio Grande do Sul (UFRGS), Porto Alegre - RS, CEP 90040-020, Brazil
https://orcid.org/0009-0007-8149-8347
carlos.dohrn@ufrgs.br

Lorenz Krefft
Hochschule München, 80333 Munich, Germany
https://orcid.org/0009-0001-0628-3326
lorenz.krefft@hm.edu

Ludwig Hoegner
Hochschule München, 80333 Munich, Germany
https://orcid.org/0000-0002-9112-3713
ludwig.hoegner@hm.edu

CC BY

Cornelius Preidel
Hochschule München, 80333 Munich, Germany
https://orcid.org/0000-0002-3573-4632
cornelius.preidel@hm.edu

Philipp Schäfer
Hochschule Mainz, 55116 Mainz, Germany
philipp.schaefer@hs-mainz.de

Florian Schill
Hochschule Mainz, 55116 Mainz, Germany
https://orcid.org/0000-0002-7463-9152
florian.schill@hs-mainz.de

Arnulph Fuhrmann
TH Köln, 50679 Cologne, Germany
https://orcid.org/0000-0001-5118-5461
arnulph.fuhrmann@th-koeln.de

SUMMARY: *3D Gaussian Splatting (3DGS) has rapidly emerged as a volumetric rendering technique that reconstructs photorealistic, real-time-navigable scenes from ordinary images or video, offering a low-cost and accessible alternative to established reality-capture methods such as terrestrial laser scanning, LiDAR, and photogrammetry. Its potential for the Architecture, Engineering, Construction and Operations (AECO) sector, however, remains underexplored. This paper combines a systematic literature review following the PRISMA 2020 guidelines with a multiple-case study to clarify the fundamentals of 3DGS and to assess its applications across the building lifecycle. Screening 4,326 unique records yielded 74 studies, which were grouped into ten application themes; cultural heritage, building reconstruction, and infrastructure currently dominate, whereas facility management, building-energy modelling, and BIM integration remain sparsely addressed. Eight complementary use cases – synthetic training-data generation for damage segmentation, construction-site documentation in virtual reality, cultural-heritage digitisation, concrete condition assessment for circular reuse, and the digitisation of a historical observatory facade – together with a dedicated 3DGS-to-IFC conversion pipeline, were analysed within a unified cross-case framework. The results indicate that 3DGS is not a replacement for geometry-centric surveying where millimetre accuracy is required, but a complementary, perception-centric representation layer that excels at photorealistic visualisation, reflective and transparent surfaces, rapid low-cost acquisition, and stakeholder communication. Beyond visualisation, 3DGS shows particular promise as an integration layer linking reality capture, BIM, and artificial intelligence, thereby supporting the next generation of potentially continuously updated, intelligent digital twins.*

KEYWORDS: *lifecycle, reality capturing, scanning, photogrammetry, 3D Gaussian Splatting, 3DGS, Scan2BIM, infrastructure, cultural heritage.*

REFERENCE: *Bartels, N., Riedlinger, U., Toubekis, G., Hagedorn, P., Herbers, P., Pinto da Silva, F., Berta Dohrn, C., Krefft, L., Hoegner, L., Preidel, C., Schäfer, P., Schill, F., & Fuhrmann, A. (2026). 3D gaussian splatting in construction – fundamentals and applications. Journal of Information Technology in Construction (ITcon), 31, 1484-1529. https://doi.org/10.36680/j.itcon.2026.060*

COPYRIGHT: *© 2026 The author(s). This is an open access article distributed under the terms of the Creative Commons Attribution 4.0 International (https://creativecommons.org/licenses/by/4.0/), which permits unrestricted use, distribution, and reproduction in any medium, provided the original work is properly cited.*

1. INTRODUCTION

Existing buildings represent one of the most valuable asset classes within the construction sector, serving as the foundation for renovation, maintenance, and management activities (Gumowski, 2025). Furthermore, cultural building heritage need to be maintained and restored (Xing et al., 2025). While in other industries digital twins (DT) are common, the condition and spatial configuration of built assets are frequently inadequately captured or outdated, despite their critical importance (Attaran & Celik, 2023; Hakimi et al., 2024). Also, the current handover processes exhibit poor information fidelity and information loss. This poses significant challenges for efficient facility management and project execution. (Cooperman & Bartels, 2026; L. Zhu et al., 2019) Accurate and up-to-date as-built documentation is essential not only for ensuring the safety and functionality of structures but also for optimizing lifecycle costs, improve performance, achieve user satisfaction and supporting sustainable construction practices (Ghansah, 2024).

Research and practice indicate a need to develop more robust systems for capturing reality to support not only construction professionals but also facility management (Anwar & Azhar, 2025; Salman & Ahmad, 2023). Currently, the predominant technologies used for capturing building geometries and conditions are Light Detection and Ranging (LiDAR) technologies, such as terrestrial laser scanning (TLS) and structure-from-motion (SfM) technologies, such as photogrammetry-based methods, e.g., for construction sites, crack detection or the capturing of built assets (Z. Chen et al., 2022; Oytun & Atasoy, 2022; Pan et al., 2022; Sestras et al., 2025; R. Yu et al., 2022; Zahs et al., 2023). While these approaches provide high-resolution three-dimensional point clouds and detailed surface reconstructions, they require substantial preparation, data acquisition time, and post-processing effort. This complexity often limits their practicality, particularly for real-time applications or scenarios demanding frequent updates. Moreover, the need for specialized equipment and expertise can lead to higher operational costs and hinder seamless integration into dynamic construction workflows. (Rábago & Portuguez-Castro, 2023; Rüter et al., 2025)

In response, emerging techniques such as Neural Radiance Fields (NeRF) and 3D Gaussian Splatting have attracted growing interest. Both are scene representation and rendering methods rather than sensing technologies: they operate on image or video data acquired with conventional cameras and reconstruct a navigable, real-time renderable representation of the scene. 3D Gaussian Splatting offers a promising alternative by enabling efficient representation and rendering of volumetric data through compact Gaussian primitives, facilitating faster data processing and potentially more flexible data acquisition strategies (Kerbl et al., 2023). By leveraging this approach, it may be possible to significantly reduce the time and complexity associated with capturing and updating as-built models, thereby improving responsiveness and decision-making on construction sites (Rüter et al., 2025).

However, despite its theoretical advantages, the application of 3D Gaussian Splatting within the construction domain remains underexplored. Key questions persist regarding its practical implementation, its integration with existing workflows, and the range of scenarios in which it can deliver tangible benefits over established methods.

This paper addresses these challenges by investigating diverse use cases for 3D Gaussian Splatting as an image-based scene representation and real-time rendering method in construction settings. Specifically, we seek to answer the following research questions:

1. Which construction-related scenarios and use cases can most effectively benefit from the adoption of 3D Gaussian Splatting compared with representations derived from traditional point-cloud acquisition methods?
2. How can 3D Gaussian Splatting be integrated within current capturing workflows to support rapid, low-effort update cycles, real-time rendering, and improved efficiency, and what trade-offs does this integration entail between visual fidelity, geometric accuracy, processing time, computational cost, interoperability, and update frequency?
3. What are the main technical and operational challenges encountered when applying 3D Gaussian Splatting in the context of building stock documentation, and how can these be mitigated?

CC BY

Through a systematic analysis and demonstration of application cases, this work aims to elucidate the potential of 3D Gaussian Splatting to transform how building assets are captured, visualized, and managed, ultimately advancing automation in construction.

2. RELATED WORK

The reconstruction and rendering of three-dimensional scenes from two-dimensional images is a fundamental problem in computer vision and computer graphics. Classical approaches such as Structure from Motion (SfM) (Schonberger & Frahm, 2016) and Multi-View Stereo (MVS) (Furukawa & Ponce, 2010; Schönberger et al., 2016) produce dense or semi-dense point clouds, which, however, require extensive post-processing for high-quality rendering. The introduction of implicit neural representations, most notably Neural Radiance Fields (NeRF) (Mildenhall et al., 2021), marked a significant paradigm shift: rather than modeling scenes through explicit geometry, a neural network encodes the scene as a volumetric radiance field and predicts color and density values for arbitrary camera poses. While NeRF achieves impressive results in novel-view synthesis, it suffers from lengthy training and inference times as well as limited editability of the scene representation. 3D Gaussian Splatting (3DGS), introduced by Kerbl et al. (Kerbl et al., 2023), addresses these limitations through an explicit, primitive-based radiance field representation. Instead of an implicit neural field, the scene is described by a set of anisotropic 3D Gaussians, each parameterized by position, covariance matrix, opacity, and spherical harmonics to model view-dependent appearance. Rendering is performed by differentiably "splatting" these Gaussians onto the image plane – a process rooted in classical point-based rendering techniques (Botsch & Kobbelt, 2003; Zwicker et al., 2002) and made real-time capable through modern graphics processing unit (GPU) rasterization. The parameters are optimized via gradient descent on reference images, while an adaptive density control mechanism dynamically adjusts the number and distribution of Gaussians throughout training. 3DGS thus combines the strengths of both worlds: the explicit, editable structure of geometry-based methods and the high visual fidelity of neural representations – while achieving substantially lower rendering times than NeRF-based approaches.

The practical application of 3DGS follows in general a three-stage capturing workflow, as illustrated in Figure 1. In the first stage, a set of overlapping images or a continuous video sequence of the target scene is recorded using standard cameras – including smartphones or action cameras – without the need for specialized hardware. The image coverage should ensure sufficient overlap between consecutive frames to support reliable feature matching. In the second stage, camera positions are estimated using Structure-from-Motion (SfM) techniques, which reconstruct approximate camera poses and an initial sparse point cloud from the image data (Schonberger & Frahm, 2016). This sparse reconstruction serves as the initialization for the subsequent 3DGS optimization, in which a set of anisotropic 3D Gaussians is iteratively fitted to the scene by minimizing photometric loss against the input images. In the third stage, the optimized Gaussian representation enables real-time rendering of novel viewpoints through GPU-accelerated rasterization, producing photorealistic images of perspectives not present in the original dataset. This pipeline thus transforms unstructured image collections into interactive, navigable 3D scene representations with comparatively low acquisition effort. It should be emphasized that no distance is measured at any stage of this pipeline. Both the metric scale and the geometric accuracy of the resulting representation are inherited from the SfM initialization, or must be introduced externally through ground control points or a reference scan.

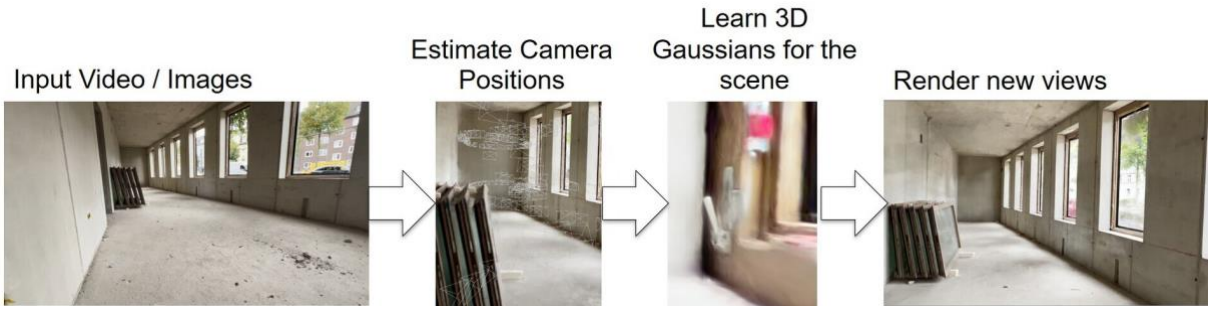


Figure 1: Capturing, learning and rendering of a 3DGS scene.

CC BY

2.1 Systematic literature review

To establish a comprehensive overview of how 3D Gaussian Splatting (3DGS) has been applied within the Architecture, Engineering, Construction and Operations (AECO) domain, a systematic mapping review was conducted and reported in line with the PRISMA 2020 guidelines (Page et al., 2021). Because the objective is to map the thematic distribution and application contexts of 3DGS in the AECO domain rather than to synthesize effect estimates, no formal quality or risk-of-bias appraisal of the included studies was performed. The review is therefore reported as a systematic mapping/scoping synthesis. The search was executed on 1 June 2026 across five bibliographic databases: Scopus, Web of Science Core Collection, IEEE Xplore, the ACM Digital Library, and Google Scholar. The conceptual query combined a technology block with an AECO application block:

> ("Gaussian Splatting" OR "Gaussian Splat*" OR "3D Gaussian*" OR "3DGS") AND ("construction" OR "building*" OR "infrastructure" OR "BIM" OR "AEC" OR "civil engineering" OR "built environment" OR "as-built" OR "scan-to-BIM" OR "reality capture" OR "progress monitoring" OR "site monitoring" OR "structural inspection" OR "defect detection" OR "facility management" OR "heritage").

Because query syntax, field codes, and wildcard handling differ between the databases, the query was translated individually for each platform. The verbatim search string per database, the searched fields (e.g. TITLE-ABS-KEY for Scopus, Topic for Web of Science, full-text metadata for IEEE Xplore and ACM DL), all applied filters (publication years, document types, language), and the number of hits per database are documented in the appendix, Table 8. Google Scholar was queried via Publish or Perish (Harzing, 2007), available from https://harzing.com/resources/publish-or-perish, with the result set capped at the first 1,000 records ranked by relevance; this cap is a known limitation of the platform and is reported as such.

The search returned 5,223 records in total (Scopus: 2,929; Web of Science: 343; IEEE Xplore: 218; ACM DL: 738; Google Scholar: 995). All records were exported in BibTeX format and imported into Zotero for deduplication. Duplicates were identified automatically by DOI, and, where no DOI was available, by an exact match of title, first author, and publication year; all automatically flagged pairs were verified manually before removal. This procedure removed 897 duplicates, leaving 4,326 unique records.

Two reviewers independently screened all 4,326 records by title and abstract. A record was retained when it both (i) genuinely concerned the 3DGS technique and (ii) addressed a construction-related application within the AECO domain. Records were excluded when they were unrelated to 3DGS or to construction, consisted of conference abstracts only, or were published in a language other than English or German. This stage removed 4,200 records, leaving 126 articles for full-text retrieval and eligibility assessment. During full-text assessment, a further 52 articles were excluded – predominantly purely methodological or fundamentals papers without a construction application, out-of-domain works (e.g. autonomous driving, robotics, or human-avatar and medical reconstruction), generic indoor or urban scene-reconstruction methods lacking an explicit AECO framing, special-case heritage outside the built environment (underwater, intangible, or artefact-level heritage), and NeRF-only studies. Screening was carried out in Zotero using a pre-defined, operationalised set of inclusion and exclusion rules, which specifies for each criterion the decision rule applied and a worked example. At the title-and-abstract stage, the two reviewers independently marked 126 and 112 records as potentially relevant, with 74 records marked by both. Across all 4,326 records this corresponds to a raw agreement of 97.9 % and a Cohen's κ of 0.61, which represents substantial agreement. Because only about 3 % of records were eligible, the chance-corrected coefficient is markedly lower than the raw agreement (prevalence-adjusted bias-adjusted kappa = 0.96); κ is reported here as the more conservative estimate. The 90 records on which the reviewers disagreed were discussed and resolved by consensus, involving a third author where no agreement was reached, resulting in 126 articles retrieved for full-text assessment. Full texts were assessed jointly rather than in duplicate, so no separate agreement coefficient is reported for this stage; 52 articles were excluded, yielding a final corpus of 74 studies. The complete selection process is summarised in Figure 2.

The 74 included studies were published between 2024 and 2026, underscoring the rapid emergence of 3DGS in the built environment. To structure the synthesis, each study was assigned to one of ten application themes; the resulting distribution is presented in Table 1. Cultural-heritage applications clearly dominate the field, accounting for 32 studies (26 on heritage documentation and reconstruction and 6 on Historic Building Information Modeling (HBIM) and heritage digital twins), followed by building reconstruction and architecture (11 studies), transportation and utility infrastructure (7), and urban digital twins (7). Structural inspection and defect detection

CC BY

(6), construction-site monitoring and process support (5) and scan-to-BIM/as-built modelling (3) represent established but smaller clusters, whereas building-energy and physical-performance modelling (2) and facility management, indoor mapping and reality-capture methods (1) remain sparsely populated – pointing to clear opportunities for future research.

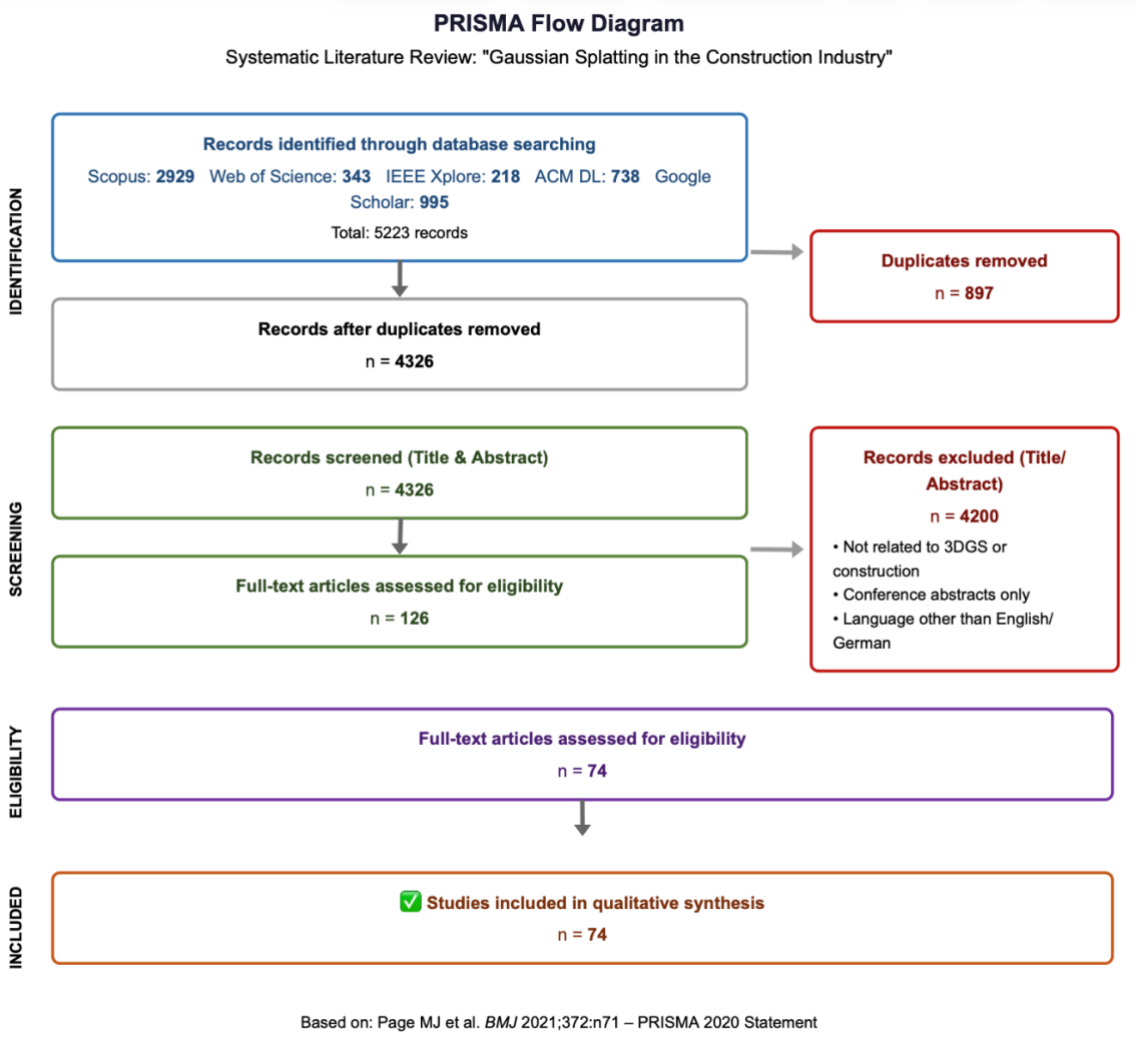


Figure 2: PRISMA 2020 flow diagram of the study identification, screening, eligibility and inclusion process.

2.2 Reality capturing in construction

A variety of sensing and reconstruction technologies are currently used to capture and model real-world environments in the AECO domain. These technologies differ significantly in terms of data acquisition principles, output representations, level of detail, and applicability. In the following, 3DGS is positioned in relation to established approaches, including LiDAR, laser scanning, photogrammetry, time-of-flight sensing, simultaneous localization and mapping (SLAM), radar, ultrasonic sensing, and general 3D scanning techniques.

Active sensor-based distance measurement technologies

Technologies such as LiDAR, laser scanning, and time-of-flight (ToF) sensors are based on active distance measurement. They emit signals (laser or light pulses) and measure the time required for the signal to return, thereby directly capturing geometric information in the form of point clouds. A prominent example in the AECO domain is terrestrial laser scanning (TLS), which represents a stationary, ground-based form of LiDAR. TLS systems are widely used for high-precision as-built documentation, deformation analysis, and heritage recording, providing highly accurate and dense point clouds (Stefańska et al., 2024).

CC BY

Table 1: Application studies of 3D Gaussian Splatting in construction, by theme (consensus set, n = 74).

Application category	n	References
Heritage – Documentation & Reconstruction	26	(Apffel et al., 2026; Barsanti & Elefante, 2026; Basso et al., 2024; Carmeliti & Marziali, 2026; Clini et al., 2024; Clini et al., 2025; Comte et al., 2024; Delgado-Martos et al., 2026; Fadilah et al., 2026; He et al., 2026; Jamil & Brennan, 2025; Jia & He, 2026; Jung et al., 2025; Lan et al., 2025; X. Li et al., 2026; A. Liang et al., 2026; Z. Liang et al., 2025; Z. Liang et al., 2026; Mirocha, 2025; Murtiyoso & MacHer, 2025; Pan et al., 2025; Qin et al., 2026; Wang et al., 2025; Wilson et al., 2025; Yu et al., 2025; X. Zheng et al., 2025)
HBIM, Heritage Digital Twins & Monitoring	6	(Kim et al., 2026; Montas-Laracuente et al., 2025; Nikolaidis et al., 2025, 2026; Suwardhi et al., 2026; J. Zhang et al., 2025)
Building Reconstruction & Architecture	11	(Cai et al., 2024; Chiappini et al., 2025; Gao, Lu, He, et al., 2025; Ham et al., 2024; Hou et al., 2025; Hu & Fukuda, 2025; Morais et al., 2024; Previtali et al., 2026; R. Wang et al., 2025; Xiong et al., 2026; Q. Zhang et al., 2025)
BIM, Scan-to-BIM & As-Built	3	(Liang, Xia, et al., 2026; Liao, Zhou, et al., 2026; Liao, Liu, et al., 2026)
Construction Site Monitoring, Process, Safety & Training	5	(Al Shafian et al., 2025; Chai et al., 2025; K. Liu et al., 2025; Rüter et al., 2025; D. Zheng et al., 2025)
Transportation & Utility Infrastructure	7	(Du et al., 2025; Du et al., 2026; S. Huang et al., 2025; J. Li et al., 2026; Ma et al., 2024; X. Wang et al., 2025; X. Wu et al., 2026)
Structural Inspection, Damage, Defect & Crack Detection	6	(D. Chen & Ma, 2026; Duan et al., 2025; Endalamaw et al., 2026; Kang et al., 2025; S. Wang et al., 2026; C.-Y. Wu et al., 2025)
Urban Digital Twins & Built Environment	7	(Do et al., 2024; Gao, Lu, Li, et al., 2025; Li, Ran, et al., 2025; W. Liu et al., 2025; X. Liu et al., 2025; Wysocki et al., 2026; H. Xu et al., 2025)
Building Energy & Physical Performance	2	(Chowdhury et al., 2026; Liang, Fang, et al., 2026)
Reality Capture, Indoor Mapping, FM & Methods	1	(Deng & Gan, 2026)
Total	**74**	

LiDAR and laser scanning are widely used for surveying, as-built documentation, and infrastructure monitoring. However, they often require specialized hardware and can be cost-intensive. Time-of-Flight sensors, commonly integrated into mobile devices, offer lower-cost and more accessible depth sensing but typically at reduced accuracy and range (Costantino et al., 2022).

These approaches generate explicit geometric representations but often lack high-quality texture information unless combined with additional imaging systems (Maru et al., 2021; Xing et al., 2025).

Image-based reconstruction approaches

Photogrammetry represents a passive, image-based approach that reconstructs 3D geometry from overlapping images using feature matching and structure-from-motion techniques (Westoby et al., 2012). It is widely used due to its flexibility and low hardware requirements e.g., standard cameras or drones (Nex & Remondino, 2014). Photogrammetry enables both geometric reconstruction and texture mapping but may struggle with reflective, textureless, or repetitive surfaces (Llull et al., 2023; Luhmann et al., 2019; Wang et al., 2024).

In contrast to active sensor-based methods, photogrammetry relies heavily on image quality and coverage, and reconstruction accuracy depends on the robustness of feature detection and matching (Wang et al., 2024; Xue et al., 2021).

CC BY

Real-time mapping and localization approaches

Simultaneous Localization and Mapping (SLAM) combines sensor data (e.g., cameras, LiDAR, or ToF) to incrementally build spatial representations while tracking the sensor position in real time. SLAM is widely used in robotics, mobile mapping, and augmented reality applications. It enables real-time operation but often produces less detailed or less globally consistent models compared to offline reconstruction methods. SLAM focuses primarily on navigation and spatial awareness rather than high-fidelity visualization (Dai et al., 2023; Li, An, et al., 2025).

Wave-based sensing technologies

Technologies such as radar and ultrasonic sensing are based on wave propagation and reflection. Radar is robust under challenging environmental conditions (e.g., dust, fog, or darkness) but typically provides low spatial resolution (Rasshofer & Geyer, 2005; Waldschmidt et al., 2021).

Ultrasonic sensors are mainly used for short-range distance measurement and object detection, with limited applicability for detailed 3D reconstruction. These methods are generally not used for high-resolution modeling but can complement other sensing technologies in specific scenarios, such as health monitoring for structures (Mutlib et al., 2016; X. Xu et al., 2024).

A comparison of the capturing methods is shown in Table 2. Here, application areas for the methods are shown as well as exemplary use cases.

Table 2: Methods for Reality Capturing in Construction with exemplary use cases, and the position of 3DGS as a representation layer.

Application Area	Capturing Methods	Exemplary Use Cases
As-Built Documentation	Photogrammetry, LiDAR, Structured Light, Multispectral Imaging	Digital building models, damage analysis
Quality Assurance	LiDAR + Photogrammetry, Ultrasound, Multispectral Imaging	Defect detection, dimensional control
Construction Progress Monitoring	ToF Cameras, SLAM, photogrammetric imaging (3DGS as representation layer)	Real-time documentation, dynamic visualization
Automated Construction Processes	SLAM, Radar, Terahertz (3DGS as representation layer)	Autonomous navigation, AI-driven control
Material and Energy Analysis	Multispectral Imaging, Ultrasound, Radar	Thermal insulation analysis, building material inspection

Positioning of 3DGS

3DGS differs fundamentally from the approaches discussed above. It is neither a sensing technology nor a point-cloud acquisition technique, but an explicit scene representation and rendering method. The scene is described by a set of anisotropic Gaussian primitives, each carrying position, covariance, opacity, and spherical-harmonics coefficients, which are optimised by gradient descent against a set of input images (G. Chen & Wang, 2025; Kerbl et al., 2023). No distance measurement takes place at any point. The method requires an upstream acquisition step – conventional images or video – and an initialisation of camera poses and sparse geometry, typically provided by Structure-from-Motion. Three consequences follow for AECO use. First, 3DGS inherits its geometric accuracy from that initialisation rather than establishing it. Second, a native 3DGS reconstruction has no absolute metric scale and no absolute coordinate system; both must be introduced externally through ground control points, known reference distances, or registration to a reference scan. Third, any point cloud derived from a 3DGS model is obtained from the centres of the optimised Gaussians and is therefore an interpretation of the optimisation result, not a set of measured points.

- In contrast to LiDAR and laser scanning, 3DGS does not measure geometry and does not directly generate metrically referenced point clouds but produces highly detailed and photorealistic scene representations.

CC BY

- Compared to photogrammetry, 3DGS offers significantly improved rendering quality and real-time rendering performance, while relying on similar image-based inputs.
- In relation to SLAM, 3DGS focuses on high-quality scene reconstruction rather than real-time localization.
- Unlike radar or ultrasonic sensing, 3DGS is not designed for robustness in adverse sensing conditions but for visual fidelity and efficient rendering.

A key advantage of 3DGS lies in its ability to combine relatively simple data acquisition (e.g., images or video) with high-quality, real-time renderable 3D representations (Kerbl et al., 2023).

However, its dependence on training processes, computational resources, and currently limited standardization poses challenges for widespread adoption in AECO practice (Rüter et al., 2025). Overall, existing technologies can be broadly categorized into active sensing methods, passive image-based reconstruction, and hybrid real-time mapping approaches. 3DGS complements these categories by introducing a novel paradigm that shifts the focus from explicit geometric reconstruction to efficient, photorealistic scene representation and rendering (G. Chen & Wang, 2025).

3. METHODOLOGY

3.1 Research design

This study adopts a multiple-case study design to investigate the application of 3DGS across a range of use cases within the architecture, engineering, construction and operations (AECO) domain. The objective is to explore how 3DGS can be adapted to different application contexts and to identify both shared patterns and domain-specific challenges. Each individual use case is evaluated independently within its specific context, considering its respective objectives, data, and methodological setup. These individual evaluations form the basis for a subsequent cross-case analysis, enabling both in-depth case-specific insights and overarching conclusions.

Given the emerging nature of 3DGS, an exploratory research approach is applied. The use of multiple cases allows for analytical generalization and supports the systematic comparison of independently developed implementations. The selected cases represent a diverse set of application domains within AEC and related fields. These include:

1. general investigations and comparative studies of 3DGS,
2. damage detection and condition assessment,
3. facility management applications,
4. cultural heritage and monument documentation (e.g., photogrammetry-based workflows),
5. sustainability-related analyses,
6. integration with artificial intelligence methods.

The selection aims to cover both technical and application-oriented perspectives, ensuring a broad representation of current research activities.

3.2 Case development, data collection and analytical framework

All cases were developed independently by different research groups, resulting in a heterogeneous set of workflows and technical implementations. While all cases are based on the same underlying principle of 3D Gaussian Splatting, they differ in:

1. data acquisition approaches (e.g., image-based, video-based, hybrid methods),
2. preprocessing and training workflows,
3. software tools and parameter settings,
4. intended application scenarios.

CC BY

The collected data includes documented workflows, generated 3DGS models, and evaluation results, which form the basis for the subsequent analysis.

To enable a systematic and transparent comparison across the heterogeneous cases, a unified analytical framework was developed. The framework was derived through an iterative process combining (i) a review of existing workflows in photogrammetry, 3DGS and AEC-related digital modeling, and (ii) an inductive screening of the initial case implementations. This dual approach ensured that both established methodological dimensions and emerging, 3DGS-specific characteristics were captured.

In a first step, common process stages were identified across all cases, including data acquisition, data processing, model generation, and application. In a second step, these stages were refined and extended based on recurring patterns and differences observed in the individual implementations. The final set of dimensions reflects both technical and application-oriented aspects relevant to the deployment of 3DGS in AECO contexts. Each case is analyzed along the following dimensions:

1. **Application context:** Description of the specific use case, including objectives, domain (e.g., damage detection, facility management, cultural heritage), and intended benefits within AEC processes.
2. **Data acquisition strategy:** Type of input data (e.g., images, video, hybrid approaches), acquisition setup, sensor characteristics, and data quality aspects.
3. **Processing pipeline and toolchain:** Preprocessing steps, training procedures, parameter configurations, and software environments used for generating the 3DGS models.
4. **3DGS model generation:** Implementation-specific characteristics of the Gaussian Splatting approach, including model structure, level of detail, and adaptation of the underlying method.
5. **Visualization and user interaction:** Rendering performance, visualization platforms, and modes of interaction, including integration into existing AEC workflows.
6. **Performance and applicability assessment:** Evaluation of the results in terms of visual quality, computational efficiency, robustness, and suitability for the intended application. Depending on the case, this includes qualitative assessments and/or quantitative indicators.
7. **Maturity level:** Classification of the development stage reached by the case, using four levels: (i) *concept* – the workflow is described and argued but not implemented; (ii) *implemented prototype* – the workflow has been implemented and executed on real data, but evaluated only qualitatively or internally; (iii) *experimentally validated* – results have been evaluated quantitatively against an independent reference or baseline; (iv) *operationally deployed* – the workflow is in routine use in a production setting. Assigning this level explicitly separates demonstrated outcomes from anticipated ones and makes the cross-case conclusions traceable to the underlying evidence (Table 6).

The framework was applied consistently across all cases using a structured documentation template to ensure comparability. At the same time, it allows for sufficient flexibility to account for case-specific characteristics and varying levels of methodological maturity.

3.3 Cross-case analysis

A qualitative cross-case analysis was conducted to systematically compare the individual cases and derive transferable insights. The analysis followed a structured, multi-step procedure based on the previously defined analytical framework.

In a first step, all cases were documented using a standardized template aligned with the analytical dimensions. This ensured a consistent level of detail and comparability across cases. In a second step, the documented cases were subjected to a within-case analysis to identify key characteristics, specific implementation choices, and case-specific outcomes.

Subsequently, a cross-case synthesis was performed by systematically comparing the cases along each analytical dimension. This involved identifying recurring patterns, contrasts, and relationships across the dataset. Particular attention was given to:

CC BY

- common patterns across application domains, such as recurring workflow structures or similar challenges,
- key differences in implementation strategies, including variations in data acquisition, processing pipelines, and toolchains,
- strengths and limitations of 3DGS in specific use cases, depending on context and requirements,
- relationships between data acquisition methods and resulting model performance, particularly with regard to visual quality, robustness, and computational effort.

The analysis was conducted using an iterative coding and grouping approach, in which observations from individual cases were progressively abstracted into higher-level categories. Emerging findings were continuously compared across cases to ensure consistency and to refine interpretations.

The analysis follows an analytical generalization logic, aiming to derive transferable insights and conceptual understandings rather than statistically representative results. This approach is particularly suitable for emerging technologies such as 3DGS, where standardized benchmarks and large-scale datasets are not yet widely available.

The diversity of methods across the cases is an intentional aspect of the study. It reflects real-world variations in research focus, technical expertise, and application requirements.

Rather than standardizing workflows, this study leverages methodological heterogeneity to better understand the flexibility and robustness of 3DGS across different domains, including engineering, cultural heritage, and AI-driven applications.

3.4 Limitations

This study is subject to several limitations. First, the heterogeneity of the cases, including differences in data acquisition methods, processing pipelines, and evaluation approaches, limits the extent to which direct quantitative comparisons can be performed. In addition, standardized evaluation metrics for 3DGS in AECO contexts are not yet established, further constraining comparability across cases. With respect to the review component, no formal quality or risk-of-bias appraisal of the included studies was conducted. The review therefore characterises the distribution and scope of the literature rather than the strength of the evidence it reports.

Second, 3DGS is an emerging technology that is still at an early stage of adoption within the AECO industry. Current applications are predominantly situated in research environments, with limited evidence of large-scale or routine use in practice. Consequently, the cases analyzed in this study primarily reflect experimental and exploratory implementations rather than fully matured workflows.

Third, the selection of cases is geographically and institutionally constrained, with a strong representation of research activities from the German-speaking academic context. While this reflects current research dynamics in the field, it may limit the generalizability of the findings to other regions or industry settings.

Finally, the number of cases is limited, and each case represents a specific application scenario. Although individual cases already demonstrate the technical feasibility and potential of 3DGS in different domains, broader validation across additional use cases and real-world projects is required. Despite these limitations, the study provides structured and systematically derived insights into the application of 3DGS across diverse contexts. The combination of independently evaluated cases and a unified analytical framework enables consistent qualitative comparison and supports the identification of transferable findings, thereby contributing to the ongoing development and future adoption of 3DGS in AECO.

4. USE CASES AND APPLICATION AREAS

Building on the analytical framework introduced in the preceding section, this section presents the individual use cases that form the basis of the multiple-case study. As outlined above, the cases were developed independently by different research groups and accordingly differ in their data-acquisition strategies, processing pipelines, toolchains, and intended application scenarios; what they share is the common principle of 3D Gaussian Splatting and a unified documentation template that ensures comparability. Together they span a broad range of AECO domains across the building lifecycle, progressing from AI-oriented data generation (synthetic training data for

CC BY

damage segmentation) through construction-site documentation in virtual reality, cultural-heritage digitisation, concrete condition assessment for circular reuse, and the capture of a historical observatory facade, to BIM-integrated navigation, superstructure inspection, and the long-term documentation of listed structures. The cases also differ in maturity. Each case is therefore explicitly assigned one of the four maturity levels defined in Section 3.2 – concept, implemented prototype, experimentally validated, or operationally deployed – stated at the beginning of the respective subsection. Section 4.10 consolidates these levels together with the input data, effort, hardware, and reported metrics of all cases in a common cross-case evidence table (Table 6), so that the cross-case conclusions drawn in Section 5 can be traced back to the evidence actually available for each case. Each case is described along the dimensions of the analytical framework – application context, data-acquisition strategy, processing pipeline and toolchain, 3DGS model generation, visualisation and user interaction, and a performance and applicability assessment – before the cross-case synthesis brings these observations together in the subsequent discussion.

4.1 3DGS for semantic segmentation

Maturity level: concept (pipeline designed and specified; no quantitative evaluation of the resulting training data reported).

The goal of this use case is to develop a pipeline for generating new training data for neural networks in semantic segmentation. The starting point is based on an existing methodology for detecting damage in three-dimensional space. In this approach, 3D point clouds are closely linked to oriented images. Damage is detected primarily in the images, then described metrically and precisely localized using the spatial information from the point cloud. At the core of this methodology is a neural network for semantic segmentation of damage in images, trained on a publicly available, already relatively diverse dataset. However, due to an existing domain gap, misclassifications still occur in practical applications. As a result, the findings currently need to be manually reviewed and corrected. Once this correction is complete, the output includes a classified point cloud with damaged areas marked. To reduce the domain gap, it is necessary to expand the training dataset with data that better reflects real-world application scenarios. However, manually creating such training data is time-consuming, costly, and prone to errors. For this reason, we propose a pipeline that enables the generation of large amounts of training data with minimal manual effort. This approach utilizes Gaussian splatting. Based on a classified point cloud, a corresponding model is generated, enabling the creation of new virtual camera perspectives within the scene. The schema is shown in Figure 3.

By combining these virtual views with the classification information from the point cloud, the generated images can be automatically annotated. This method enables the efficient expansion or creation of a domain-specific training dataset. The expected benefits are:

- Reduction in manual annotation efforts
- Scalable generation of large training datasets
- Improved model performance through domain-specific data
- Reduction in costs and error rates

3D Gaussian Splatting (3DGS) was chosen because it enables the generation of nearly photorealistic images of a scene in (near) real time. A key advantage of this method is its high level of detail: even fine structures such as cracks or minor damage are preserved in the generated images. This is particularly crucial for the semantic segmentation of damage.

Another key advantage of 3DGS is its relatively small domain gap. Since the model is reconstructed directly from real-world data (e.g., point clouds and images), the visual characteristics of the target domain are largely preserved. As a result, the generated training data is significantly closer to real-world use cases than with purely synthetic approaches.

CC BY

Alternatives and their limitations are as followed:

- Traditional synthetic data generation (e.g., rendering in game engines): While these methods allow for a high degree of control over scenes, they often exhibit a significant domain gap, as materials, lighting, and surface textures do not exactly correspond to reality.
- Neural Radiance Fields (NeRF): NeRF-based approaches also offer high visual quality but are typically more computationally intensive and less efficient at generating large amounts of data or new perspectives than 3DGS.
- Direct projection of labels from point clouds onto existing images: Although this approach is easy to implement, it does not allow for the generation of new camera perspectives. The resulting data diversity is therefore severely limited and is often insufficient to effectively reduce the domain gap.

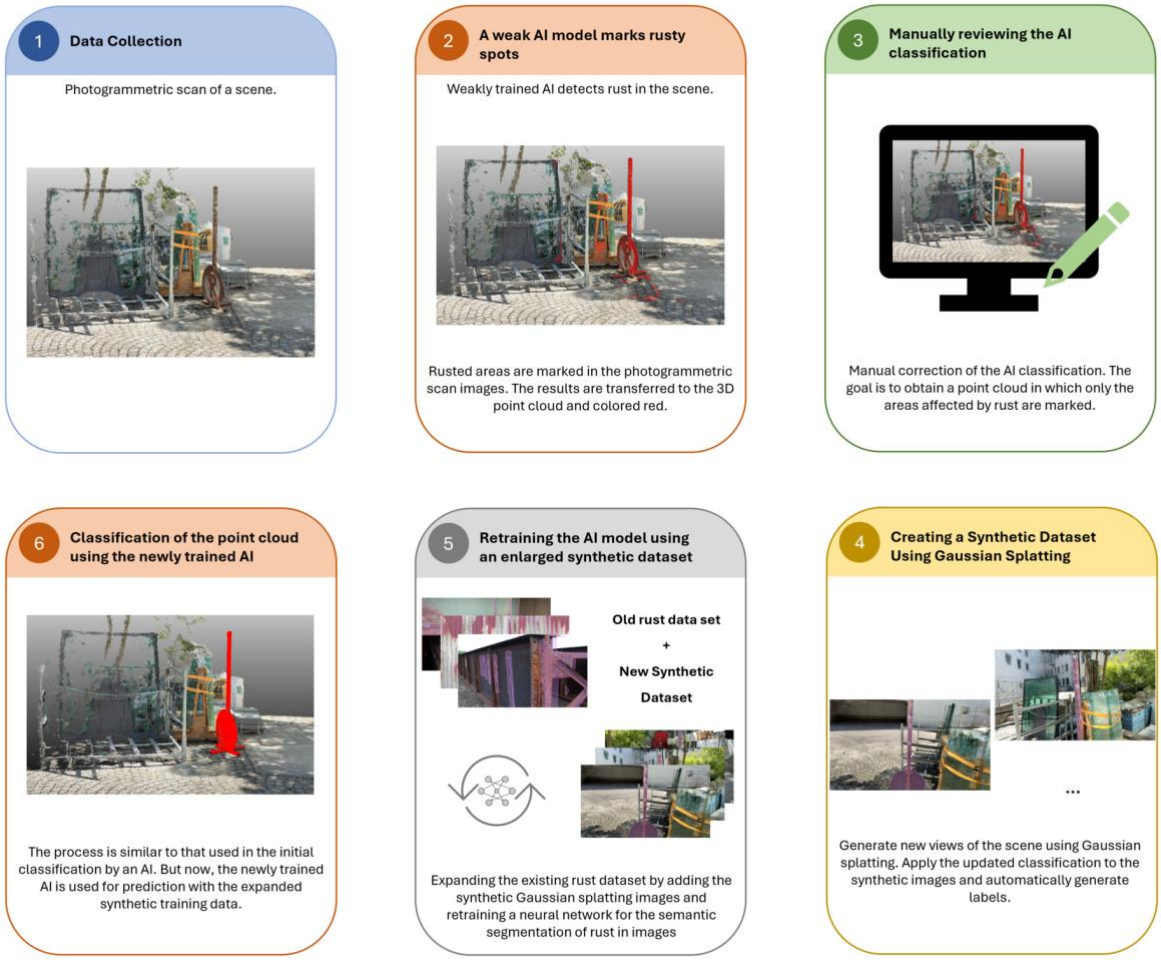


Figure 3: Schema for classifying, training and creating synthetic datasets using 3DGS.

Compared to these alternatives, 3DGS thus offers the best combination of:

- High visual quality
- Preservation of fine geometric details
- Efficient generation of new views
- Low domain gap

CC BY

Based on this, the processing Pipeline and Toolchain was designed as follows:

4. Photogrammetric recording and reconstruction of a scene: Capturing the real-world environment and generating a 3D point cloud and corresponding oriented images.
5. Damage analysis and manual post-processing: Analysis of the scene for damages, as well as manual correction and classification in accordance with the methodology described in (Krefft & Hoegner, 2025)
6. Construction of the 3D Gaussian Splatting Representation: Creation of a 3DGS model based on the reconstructed data using the following approach "3D Gaussian Splatting for Real-Time Radiance Field Rendering". (Kerbl et al., 2023)
7. Generating new camera perspectives: Rendering additional virtual views of the scene from different perspectives.
8. Automatic label generation: Transferring the damage classification from the point cloud to the newly generated images to create annotated training data.

Table 3: Comparison of different capturing technologies for technical building equipment.

Technology	Scene 1 - detail	Scene 2 - room scene
3DGS		
Terrestrial Laser Scanner		
Photogrammetry		
LiDAR		

4.2 3DGS for construction sites

Maturity level: experimentally validated for the beam and room scenes (TLS/MLS reference); implemented prototype for the four site scenarios, which were assessed qualitatively only.

Capturing the realities on construction sites is important for quality control, as-built documentation as well as project management and construction progress monitoring (ElQasaby et al., 2022; Grogan et al., 2022; Sami Ur Rehman et al., 2022). Therefore, this use case focuses on capturing construction-site environments using 3DGS and visualizing them on desktop computers and in Virtual Reality (VR). Four representative construction scenarios were investigated: a shell apartment and a reinforcement cage as well as technical building equipment in a detail scene and a room scene. The primary aim is to create highly realistic digital twins from simple video recordings, enabling virtual site inspections, progress documentation, reinforcement verification, stakeholder communication,

CC BY

and presentation of construction progress. Expected benefits include reduced site visits, faster documentation, improved understanding of complex construction conditions, enhanced collaboration among project participants, and support for skilled-labor shortages through improved remote access to site information.

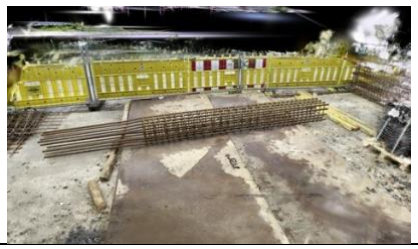
3DGS was selected because it provides photorealistic scene reconstruction with significantly higher visual quality than conventional image-based methods while requiring only video recordings as input. Compared with traditional laser scanning and LiDAR approaches, 3DGS offers a faster and more accessible workflow.

The workflow started with video capture using smartphones equipped with an ultra-wide-angle camera (4K resolution, 60 fps). Consistent exposure, fixed focus, and smooth camera movements were essential for reconstruction quality. The captured data were processed using either the open-source 3DGS implementation by Kerbl et al., Polycam's cloud-based reconstruction service or Kiri Engine.

The comparison demonstrated that 3DGS achieved the highest reconstruction quality, capturing fine details such as reinforcement wires and construction elements with near-photographic realism. Comparing the technical building equipment scenes, KIRI engine had the best results. A comparison of 3DGS to other capturing technologies for technical building equipment is shown in Table 3. The scenes were captured in 2026.

Table 4 shows the results for the comparison on construction sites, that were captured in 2024.

Table 4: Comparison of different capturing technologies in construction according (Rüter et al., 2025).

Technology	Scene 1 - view	Scene 2 - detail
3DGS Kerbl et al.		
Splatting via Polycam		
Photogrammetry via Polycam		

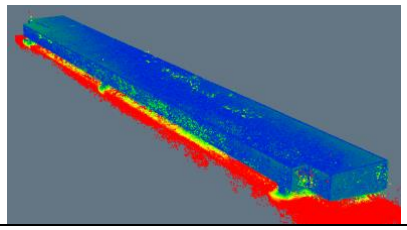
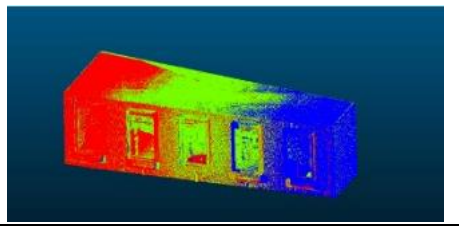
Polycam Gaussian Splatting delivered slightly lower quality but required less specialized hardware and offered easier deployment. Photogrammetry generated much smaller file sizes and simpler models but suffered from missing details, artifacts, and reduced depth perception. Processing times ranged from approximately 30–90 minutes for Kerbl's implementation and 30–60 minutes for Polycam in the capturings in 2024. The main limitation of high-quality 3DGS models were their large data volume and demand for powerful graphics hardware. Compared with traditional reality-capturing approaches such as laser scanning, 3DGS offers a promising balance between quality, speed, accessibility, and immersive visualization, making it particularly suitable for construction documentation and communication workflows.

CC BY

Regarding the quantitative accuracy data, results from a recent comparative study on 3DGS geometric accuracy are summarized below. In the first study (capturing of a beam), unfiltered 3DGS reconstructions deviated substantially from the TLS reference (58.7 mm deviation, 15.1 mm variance), an error attributed primarily to the missing absolute scale of SfM-initialized reconstructions rather than to the splatting process itself. After opacity-based filtering (removing Gaussians with ≤50% opacity) and ICP-based rescaling, deviation dropped to 5.3 mm (variance 10.5 mm, a 90.9% reduction) closely matching the MLS benchmark of 6.4 mm (variance 9.8 mm). Qualitatively, 3DGS was the only method able to resolve fine surface detail such as concrete pores and spalling, information not retrievable from the sparser MLS point cloud, although structural deflection remained detectable only in the TLS reference due to its higher point density.

For the second study (room scene), C2C distance analysis in CloudCompare yielded a standard deviation of σ = 71.3 mm (unfiltered) across the full room, and 25.3 mm after filtering. Normalized against each principal dimension ($\delta_i = (\sigma/D_i) \times 100$), this corresponds to just 0.43% of the room's 16.710 m length but rises to 1.86–3.56% along the narrower, non-parallel Y-dimension and 2.55% of the 2.800 m room height, illustrating the scale-dependence of relative geometric accuracy. A direct dimensional check of the same 16.710 m wall yielded ΔL = 0.028 m (0.17%, ≈1.68 mm/m) — roughly 2.55× smaller than the C2C standard deviation, since C2C captures spatial variability across the full point cloud while the dimensional check evaluates a single macroscopic measurement. Table 5 summarizes these results, illustrating both the achievable accuracy of filtered/rescaled 3DGS reconstructions and the scale-dependent nature of relative geometric error.

Table 5:Quantitative geometric accuracy of 3DGS reconstructions.

Metric	Scene 1 (beam)	Scene 2 (room)
Visual C2C result		
Reference dimensions [m]	X: 8.847 / Y: 0.956 / Z: 0.769	X: 15.840–16.710 / Y: 2.005–3.835 / Z: 2.800
Deviation, unfiltered 3DGS [mm]	58.7 (var. 15.1)	71.3
Deviation, filtered + ICP-rescaled 3DGS [mm]	5.3 (var. 10.5)	25.3
Reduction through filtering	90.9%	
MLS benchmark [mm]	6.4 (var. 9.8)	
Normalized deviation δ (per dimension)		0.43% (X) / 1.86–3.56% (Y) / 2.55% (Z)
Direct dimensional check ΔL		0.028 m (0.17%, ≈1.68 mm/m)

Beyond processing time, a systematic quantitative comparison across the investigated construction scenarios in this chapter remains methodologically challenging. Unlike the concrete-beam and room-scene studies discussed in this section, no co-registered ground-truth reference (e.g., TLS or MLS) was captured for these four scenarios, so reconstruction quality could only be assessed qualitatively through visual inspection rather than through metric deviation values. This reflects a broader challenge in evaluating 3DGS for construction documentation: rigorous accuracy assessment requires an independent high-precision reference dataset captured under comparable conditions, which is rarely available in practice-oriented, time-constrained site documentation workflows. Establishing such reference datasets, even for a subset of representative scenes, is recommended for future work to enable direct quantitative benchmarking of 3DGS against traditional capturing technologies within the same construction-site context.

CC BY

4.3 Combining IFC and 3DGS

Maturity level: implemented prototype (end-to-end pipeline executed on a single room; semantic and topological validity assessed, no independent geometric or schema validation).

This section presents the implementation of a processing pipeline that transforms 3DGS representations into structured, BIM-compatible models based on IFC. The workflow integrates volumetric scene representations with conventional geometry-based processing and semantic modeling approaches, combining established software environments with custom-developed Python scripts.

The process begins with the generation of a 3DGS scene representation, which provides a visually rich and robust reconstruction of indoor environments. However, due to its implicit and view-dependent nature, the 3DGS representation is not directly compatible with BIM-oriented workflows. Therefore, an intermediate transformation into a point-based representation is required. During this conversion, the original 3DGS model is reduced to its geometric core, retaining spatial coordinates and surface normals, while advanced radiometric properties such as view-dependent color encoded through spherical harmonics are not preserved. This highlights a fundamental interoperability gap between radiance field rendering approaches and established BIM processing paradigms.

Following the conversion, the resulting point cloud undergoes a series of processing steps to ensure geometric consistency and suitability for further modeling. This includes spatial alignment to a consistent coordinate system, noise reduction, and segmentation into structurally meaningful elements such as walls, floors, openings, and other building components. Due to the characteristics of 3DGS-derived data, such as uneven point density, limited edge sharpness, and partial discontinuities, geometry-based segmentation strategies are applied to reliably distinguish structural elements.

To address incomplete surface coverage caused by occlusions during data acquisition, a surface completion step is introduced. This step employs a custom algorithm that combines planar fitting, convex hull computation, and interpolation to generate additional points within the boundaries of segmented elements. The objective is not to increase geometric detail, but to ensure topological completeness and stable surface definitions for subsequent processing.

Following surface completion, a voxel-grid-based downsampling approach is applied to reduce redundancy while preserving geometric structure. This step ensures a uniform point distribution and significantly reduces data volume, resulting in an optimized representation that balances geometric fidelity and computational efficiency. The combination of surface completion and controlled downsampling leads to a structurally consistent point cloud that is well suited for geometric abstraction.

A key component of the workflow is the transformation of point-based representations into simplified geometric models. Instead of relying on conventional mesh reconstruction techniques that approximate surfaces through dense triangulations, a rule-based abstraction approach is applied. Planar elements are identified and approximated through fitted planes, from which 2D contours are derived and subsequently extruded into volumetric mesh representations. This results in a highly reduced geometric model that captures the essential spatial characteristics of building elements while minimizing complexity.

The resulting mesh elements are exported and further processed for integration into Building Information Modeling (BIM) environments. A custom Python-based toolchain is used to convert the geometric data into the Industry Foundation Classes (IFC) format. This process includes automated classification of elements based on naming conventions and geometric properties, the generation of a hierarchical BIM structure (project, building, storey, elements), and the establishment of semantic relationships between elements, such as the integration of openings into wall structures. Geometric information is incorporated using triangulated mesh representations, ensuring compatibility with standard BIM viewers.

The final IFC model represents a semantically structured but geometrically simplified building model. The level of development corresponds approximately to LOD 200 for planar building elements, as the model captures overall geometry and spatial relationships but does not include detailed material, structural, or performance-related attributes.

The workflow is shown in Figure 4 and shows the conversion from a 3DGS into an IFC-file.

CC BY

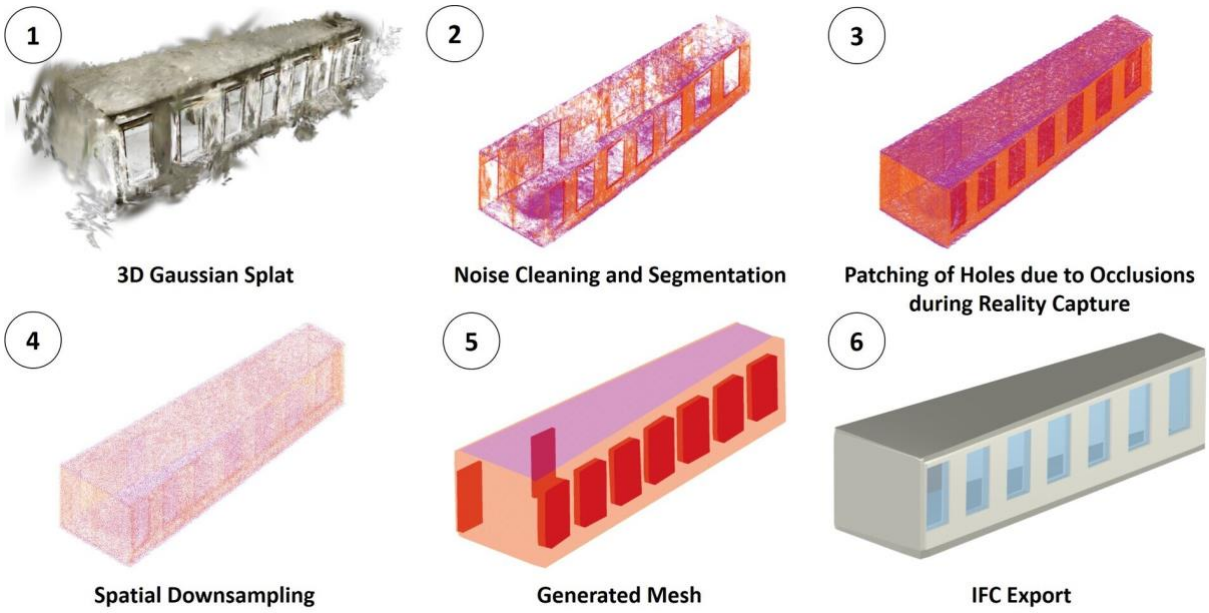


Figure 4: Pipeline for converting 3DGS into IFC models.

The main contribution of this implementation lies in the development and demonstration of an end-to-end pipeline that bridges the gap between 3DGS and BIM-based modeling. Specifically, the workflow (i) enables the transformation of implicit 3DGS representations into explicit, BIM-compatible geometries, (ii) introduces a geometry-aware abstraction strategy tailored to planar building elements, and (iii) integrates automated semantic structuring within the IFC framework. By combining data-driven reconstruction with rule-based geometric and semantic processing, the approach provides a novel pathway for incorporating emerging 3DGS scene representations into established AECO workflows. Building on the eight-stage pipeline architecture introduced above (Figure 4), the following details the underlying methodological parameters, thresholds, and evaluation results for each stage, as documented in the accompanying implementation study underlying this paper (Bartels et al. 2026).

The raw point cloud (2.6M points) is manually aligned to a consistent coordinate frame and progressively cleaned of gross and interior noise, yielding 1.6M points prior to segmentation. Several automated segmentation methods (Statistical/Radius-based Outlier Removal, Region Growing, Distance/Density-based Clustering, Plane Detection, and a PointNet++ model pretrained on S3DIS) were evaluated but proved unreliable due to the uneven point density and weakly defined edges characteristic of 3DGS-derived data; segmentation was therefore performed manually rather than via threshold-based rules, yielding 15 semantically labelled segments (2 floors, 4 walls, 7 windows, 2 doors; 1.3M points). Occlusion-induced gaps were closed via SVD-based plane fitting, convex-hull computation, and grid interpolation at 10 mm spacing (2.65M points), followed by voxel-grid downsampling at 50 mm spacing (69.7K points) as a compromise between geometric fidelity and computational cost. Segments were converted into prismatic meshes (230 vertices, 400 triangles) via PCA-based plane fitting and contour extrusion, then processed by a custom ifcOpenShell-based generator targeting IFC4.3 (ISO 16739-1:2024), which constructs the standard spatial hierarchy and derives entity classification (e.g., IfcWall, IfcWindow) and opening relationships (IfcRelVoidsElement/IfcRelFillElement) from segment names. The resulting geometry corresponds to LOD 200, providing approximate shape, size, and location for each element but no material, structural, or performance-related attributes.

The pipeline achieved a 12,000:1 point-reduction ratio and 100% semantic classification accuracy, a figure that follows directly from the manual nature of the segmentation step rather than from an independently validated classifier. The resulting IFC file loaded without reported errors in BIMCollab Zoom, though no formal schema validation (e.g., via the buildingSMART Validation Service) was performed. Processing required approximately 1 hour per room, with segmentation alone accounting for roughly 80% of this time. Three limitations affect robustness: the convex-hull-based patching step tends to re-close previously segmented openings such as windows, requiring re-segmentation or a revised processing order; the mesh-generation approach assumes planar elements

CC BY

of uniform thickness and does not extend to curved or non-planar geometry; and validation was conducted on a single room, so generalizability to larger or more complex buildings remains untested. Two aspects requested for full methodological transparency could not be addressed within the scope of the underlying study and are noted as open points: the method used to derive surface normals during point-cloud import was not documented, and no geometric-error assessment (e.g., cloud-to-cloud comparison against an independent TLS or MLS reference) was performed on the final IFC geometry, as the study focused on semantic and topological validity rather than metric accuracy.

Overall, the implementation demonstrates that 3DGS-derived scene representations can be systematically transformed into BIM-compatible models through a structured processing pipeline. While the workflow requires abstraction and reduction of the original data, it enables the integration of volumetric rendering outputs into established AECO processes and highlights the potential of 3DGS for efficient data acquisition and reconstruction in BIM-oriented applications.

4.4 3DGS in the cultural heritage sector

This subsection is a state-of-the-art synthesis of the heritage domain rather than an independent case of this study and is therefore not assigned a maturity level.

The earliest application of splat-based rendering to cultural heritage arose directly from a documentation problem of scale. The Digital Michelangelo Project of Stanford University (Levoy et al., 1999) produced a two-billion-polygon laser scan dataset of Michelangelo's David – a dataset that exceeded the display capacity of conventional rendering pipelines at the time of acquisition (Levoy et al., 2000). The QSplat rendering system (see Figure 5) was developed to make this data navigable in real time, projecting point-cloud geometry as screen-space splats within a multiresolution bounding-sphere hierarchy (Koller et al., 2004; Rusinkiewicz & Levoy, 2000, 2001).

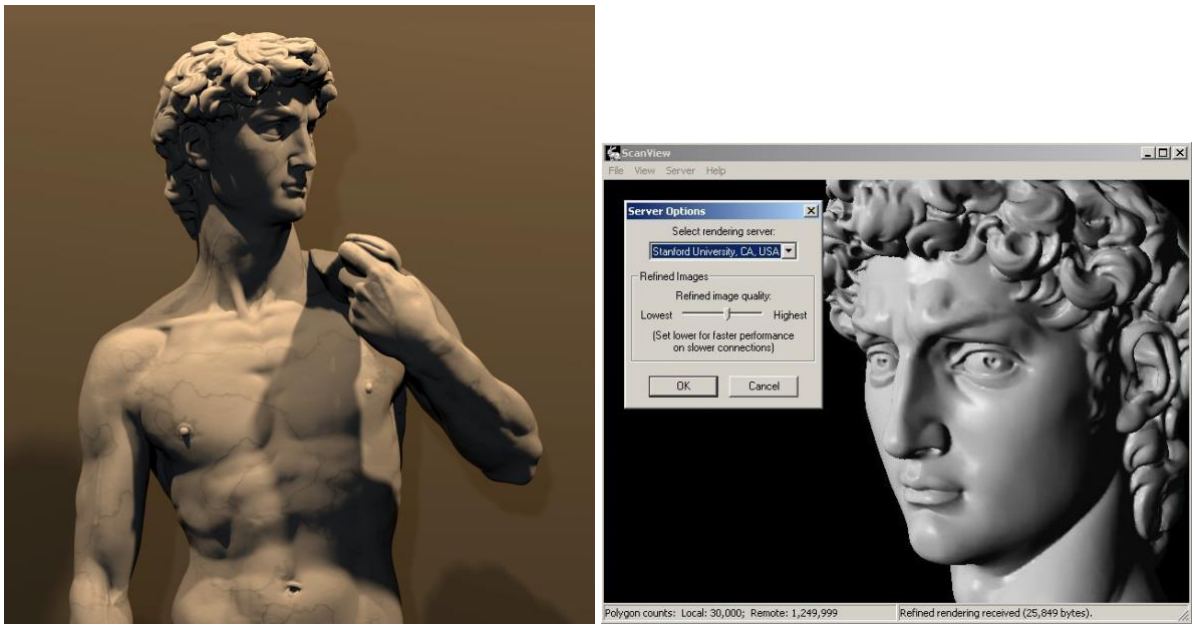


Figure 5: The 3D Michelangelo project and QSplat rendering system (Image: Stanford University/ Soprintendenza ai beni artistici e storici per le province di Firenze, Pistoia, e Prato).

Refinement of this approach into the Elliptical Weighted Average (EWA) framework improved handling of the anisotropic surface characteristics common to scan-derived heritage data (Zwicker et al., 2001), and GPU-accelerated implementations established real-time display of large heritage point clouds as a practical capability (Botsch et al., 2005; Kobbelt & Botsch, 2004).

Image-based 3D modelling established itself as the standard photogrammetric workflow for heritage documentation through the 2000s and 2010s, producing metric-accurate dense point clouds and textured meshes from multi-image capture campaigns (Remondino, 2011; Remondino & El-Hakim, 2006; Stylianidis et al., 2016).

CC BY

For sites with complex access constraints, dense surface ornamentation, or requirements for real-time interactive presentation, however, these workflows remained computationally intensive and produced outputs primarily suited to offline analysis and archival use (Santagati et al., 2013).

Neural Radiance Fields (NeRF) (Mildenhall et al., 2021) introduced a complementary approach: photorealistic navigable scene representations synthesised directly from image collections, without a mesh intermediary. For heritage sites where novel-view synthesis and immersive public presentation were primary documentation goals, evaluations conducted at the 29th CIPA Symposium in Florence (2023) identified NeRF as a viable method (Mazzacca et al., 2023). The NeRFBK benchmark dataset, assembled from heritage objects, provided open evaluation infrastructure against which NeRF implementations could be systematically compared (Yan et al., 2023). Benchmarking across objects of varying texture, reflectance, and surface complexity identified geometric accuracy as a limiting factor: NeRF outputs did not meet the precision requirements of metric-critical documentation tasks, a constraint that photogrammetric workflows did not carry (Remondino et al., 2023).

3D Gaussian Splatting (3DGS) (Kerbl et al., 2023), published at SIGGRAPH 2023, addressed the rendering speed limitations of NeRF while retaining novel-view synthesis capability. The method derives differentiable 3D Gaussian primitives from a Structure-from-Motion (SfM) point cloud, refines them from multi-view images, and renders the result in real time via GPU-accelerated alpha blending. For heritage practitioners, this represents a workflow compatible with established photogrammetric acquisition practice – image capture, SfM processing, and direct rendering – while producing immediately navigable scene outputs without a mesh intermediary. Comparative evaluation has confirmed, however, that 3DGS shares with NeRF a fundamental constraint for metric-critical documentation: SfM-MVS retains superior geometric precision where dimensional accuracy is a primary requirement, a limitation attributable in part to multi-view inconsistency in the Gaussian primitive representation (Clini et al., 2024; B. Huang et al., 2024).

The precision gap identified above has prompted documentation workflows that draw on two complementary methods: Terrestrial Laser Scanning (TLS) for metric accuracy, and splat-based rendering for real-time visual output. This combination has antecedents before 3DGS: at Aachen Cathedral (UNESCO World Heritage Site), splat-based rendering with plane fitting was applied to TLS point clouds of the historic timber attic to derive models for finite element structural simulation (Selman et al., 2022), establishing the paired use of metric scan data and splat-based rendering as a viable heritage documentation approach. Direct comparative evaluation across heritage sites in Palermo and at the Church of Santa Maria della Piazza in Ancona (2024) characterised 3DGS capabilities and constraints across a range of heritage documentation tasks (Basso et al., 2024; Clini et al., 2024). The multi-view inconsistency described above was partially addressed by 2D Gaussian Splatting (2DGS, SIGGRAPH 2024), which reconstructs surfaces through oriented planar Gaussian primitives rather than volumetric ellipsoids (B. Huang et al., 2024). By 2026, documented heritage practice has increasingly addressed the precision–fidelity trade-off through hybrid acquisition strategies rather than methodological substitution. In this approach, the metric accuracy of TLS is combined with the high-fidelity visual rendering capabilities of 3DGS, both for heritage building documentation and for UAV-based urban heritage surveys where ground-level access is limited or impractical (Fadilah et al., 2026; Suwardhi et al., 2026). These developments position the cultural heritage domain as a testbed for novel and innovative application scenarios.

4.5 3DGS for assessing the condition of concrete elements for circular reuse

Maturity level: implemented prototype (workflow executed on dismantled elements; damage detection and IFC enrichment demonstrated, no quantitative accuracy evaluation).

In the context of circular reuse of cast-in-place concrete elements, a Pre-Demolition Audit (PDA) is a systematic, ex-ante assessment of a building prior to (selective) dismantling, with the objective of identifying, quantifying, and characterizing materials, elements, and hazardous substances to enable circular reuse (European Commission, 2018). Within this process, the on-site inspection represents the empirical data acquisition phase, encompassing the in-situ observation, documentation, and measurement of building elements, materials, and damage patterns. It traditionally relies on manual surveys, photographic documentation, and expert judgment, but increasingly incorporates digital capture techniques (Rašković et al., 2020), e.g. previous approaches use laser scanning and other data capturing technologies for the resources asessment (Gordon et al., 2024; Xiong et al., 2022), while a comparison between the application of 3DGS and Laserscanning has been provided in literature showing that while laserscanning offers great precision, the ease of use, low-cost equipment, and processing time of 3DGS has

CC BY

been advantageous to the capturing and asessment process (Hagedorn et al., 2026). Condition assessment is usually done in two steps: first, before dismantling in the PDA; and second, in the dismantled state of the elements, to conduct more detailed tests.

Against this background, the present use case addresses the acceleration of PDAs and condition assessment for reinforced concrete structures through the application of 3DGS. The use case is demonstrated on already dismantled cast-in-place elements from a university building at Ruhr University Bochum. Conventional approaches to on-site inspection and material inventory generation are often time-consuming, prone to subjectivity, and limited in their spatial and semantic resolution, particularly when complex damage phenomena such as cracking, spalling, or corrosion must be assessed. The proposed approach (see Figure 6) integrates image-based scene reconstruction into the audit workflow by capturing video sequences and targeted image sets of the structure, including detailed recordings of damage features. These data are processed using 3DGS to generate a dense, radiance-based representation of the scene, enabling efficient rendering and spatially coherent visualization. The scene rendering is done in *Postshot by Jawset (v0.6.150)* with Splat3 radiance field profile and maximum splat count setting of 3000k, and 30k training steps with anti-aliasing enabled.

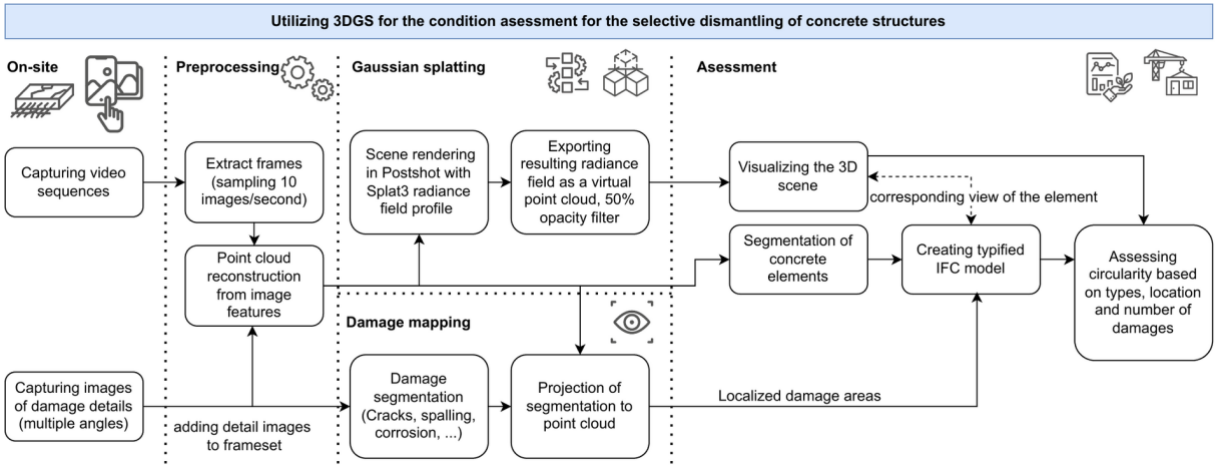


Figure 6: Overview of the application of 3DGS for the pre-demolition audit for selective dismantling of concrete structures.

Additional detail images that are captured during the audit are analyzed using a damage segmentation algorithm (e.g. as introduced in (Çelik et al., 2024) to detect cracks, spalling, corrosion and honeycombs on concrete surfaces). Figure 7 shows an example of a detected spalling area on a concrete element.



Figure 7: Left: Gaussian splat of a cast-in-place concrete element. Right: Damage detection of spalling on the same element.

The detail images are then mapped onto the point cloud using the approach by (Herbers et al., 2025), where individual points are assigned a damage class. Figure 8 shows the reconstructed point cloud with classified damage areas. The annotated point cloud can then provide damage location and classification, as well as size and volume metrics.

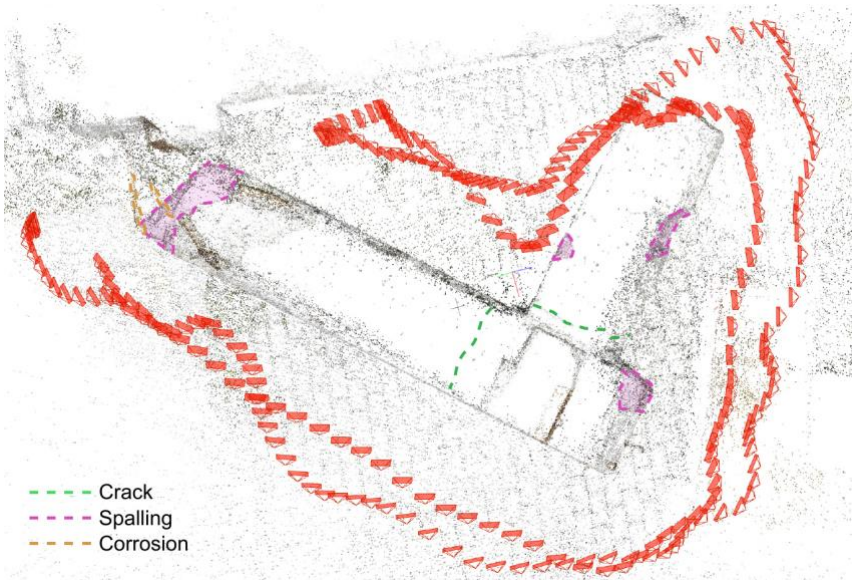


Figure 8: Point cloud reconstruction of the video inspection (top down view). The camera trajectory is displayed in red. Cracks, spalling and corrosion areas are detected in the video material and then projected onto the point cloud.

The concrete elements are segmented and subsequently transformed into a typified Industry Foundation Classes (IFC) model, in which geometric entities are enriched with semantic attributes such as material classification, condition state, and damage characteristics. This semantically enriched model enables the automated or semi-automated derivation of a material inventory, including quantitative information and condition-dependent recovery potentials, which in turn supports the assessment of circularity and the planning of selective dismantling strategies.

This use case aims to demonstrate a 3DGS-based methodology to enhance the efficiency, accuracy, and BIM integration of concrete condition assessment (e.g., for PDAs and circular reuse) through video-based data acquisition, high-resolution reconstruction, and IFC-based workflows. The approach reduces inspection time, improves early data quality and automation, and generally supports sustainable development goals with circular construction by enabling more precise material assessment and optimized dismantling planning.

4.6 3DGS for capturing historical landmarks - astronomical observatory facade in 3DGS

Maturity level: experimentally validated (quantitative comparison against a Z+F Imager 5010C TLS reference, single campaign).

The building of the Astronomical Observatory of the Federal University of Rio Grande do Sul (Porto Alegre, Brazil), inaugurated in 1908, was restored and designated as a historical heritage site in 2002. Currently, it hosts free activities for the community, including guided tours of its museum, sky observation, and workshops aimed at schools and the general public. Considering the historical and educational importance of this building, the three-dimensional digitization of its main facade using the 3D Gaussian Splatting (3DGS) technique can contribute to its preservation and the promotion of its activities, especially through photorealistic visualization. Furthermore, the high fidelity in capturing surface details makes it a promising tool for remote inspections and the identification of historical degradation patterns. By providing a detailed digital snapshot at a specific point in time, this technique enables future comparisons, allowing for longitudinal monitoring of structural decay and assisting in the planning of restoration interventions. Digitization via 3DGS was chosen because it provides high-end photorealistic results quickly using consumer-grade equipment, such as mobile phones or conventional cameras, with significantly lower computational overhead for real-time rendering than alternatives like NeRF (Neural Radiance Fields). Conversely,

CC BY

terrestrial laser scanners and structured light systems offer lower quality in capturing transparencies and reflective surfaces — a limitation shared by photogrammetry — despite their superior nominal geometric precision. Additionally, both types of scanners, especially laser scanners, typically involve substantially higher equipment costs. The data for the 3DGS was captured using an iPhone 15 Pro Max assisted by a DJI Osmo Mobile 3 gimbal for image stabilization to minimize motion blur. The SplatKing app was used as it enables fixed camera parameter settings and the simultaneous capture of photo sequences with two lenses. Thus, based on the ambient lighting conditions, the ISO, shutter speed, and white balance were adjusted and locked. A total of 462 photos were taken: 231 with the wide lens (25mm) and 231 with the ultra-wide lens (14mm). The shooting process began at the furthest point from the facade, moving laterally along it and gradually approaching at different heights. The image alignment process and COLMAP export were performed using RealityScan v2.1.1 software. The Gaussian Splatting training was conducted in LichtFeld Studio v0.5.1, limited to 3 million Gaussians and using degree 3 spherical harmonics (SH), as illustrated in Figure 9. The generated PLY file was then imported, cleaned, and exported in its final version via the SuperSplat online platform. All software used is free for academic purposes.



Figure 9: 3DGS training in LichtFeld Studio software, showing the positions from which the photographs were taken.

The photorealistic 3DGS model of the Astronomical Observatory enables diverse applications by combining high-fidelity visualization with interactivity. For this use case, the model is designed for integration into game engines and web-based platforms, offering interactive viewing from multiple angles and distances. Such resources can be hosted on official university websites for educational purposes or used in the pre-production of audiovisual projects, serving as a versatile tool for both heritage preservation and institutional promotion. Furthermore, from a construction management perspective, it offers a significant advantage in monitoring structural pathologies; unlike traditional point clouds, its view-dependent reflections and dense volumetric representation facilitate the visual detection of moisture stains, hairline cracks, and material weathering. This allows experts to perform preliminary visual assessments without the immediate need for scaffolding or high-end metrological equipment.

CC BY

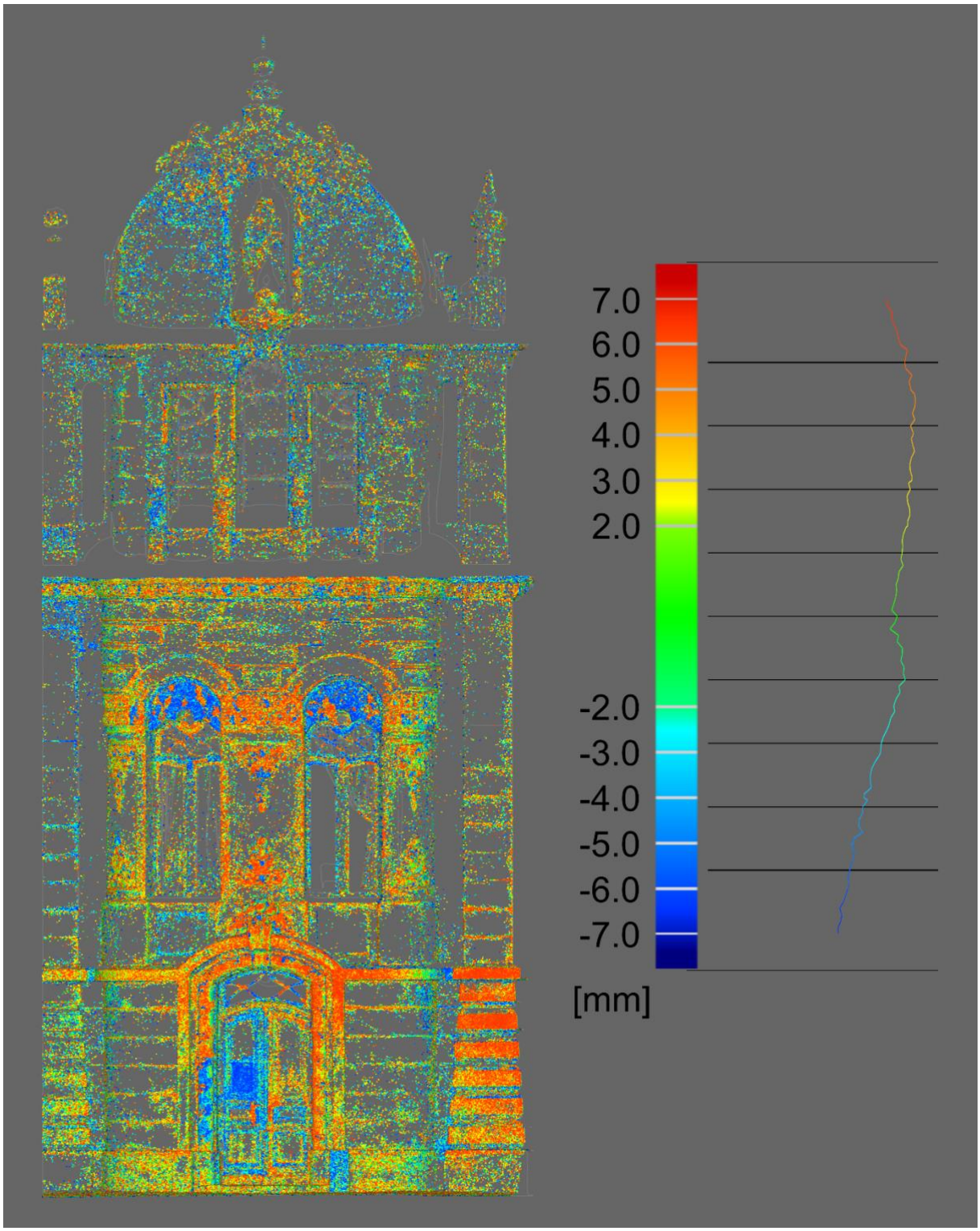


Figure 10: 3D deviation analysis of the 3DGS point cloud relative to the laser scanner.

The 3DGS facade digitization underwent quantitative, qualitative, and performance comparisons with a reference digitization performed using a Z+F Imager 5010C terrestrial laser scanner. The acquisition was conducted from three scan positions: one central station point further from the facade, and two closer positions at 45° angles relative to the first. This equipment was chosen because it offered the highest geometric precision among those available

CC BY

for use. In terms of performance, the 3DGS technique required 8 minutes for image capture, 3.5 minutes for alignment, and 55 minutes for model training, totaling approximately 66.5 minutes. The laser scanner workflow took 45 minutes for scanning, 10 minutes for setup, and 20 minutes for processing in Autodesk Recap 2026 software, totaling approximately 75 minutes. The same workstation was used for the data processing of both methods, featuring an Intel i9-13900F CPU, 128GB of RAM, and a GeForce RTX 4070 GPU (12GB VRAM). After cleaning the data, the 3DGS point cloud (2 million points) and the laser scanner point cloud (14.6 million points) were imported into Geomagic Wrap software for quantitative and qualitative comparative analysis. Since native 3DGS produces unscaled reconstructions due to the lack of metric Ground Control Points (GCPs), a manual scaling procedure was applied. Physical field measurements of the main entrance door width (2.08 m, taken via steel tape measure) were used to compute a resulting scale factor of 0.3389. To ensure metric consistency, this distance was cross-verified against the laser scanner point cloud, which yielded a corresponding width of 2.082 m, confirming high dimensional agreement (relative error of 0.09%) with the reference dataset. Regarding control measurement uncertainty, the reference TLS dataset was acquired with a nominal range noise of 0.4 mm RMS at 10 m and a linear accuracy of ≤ 1 mm.

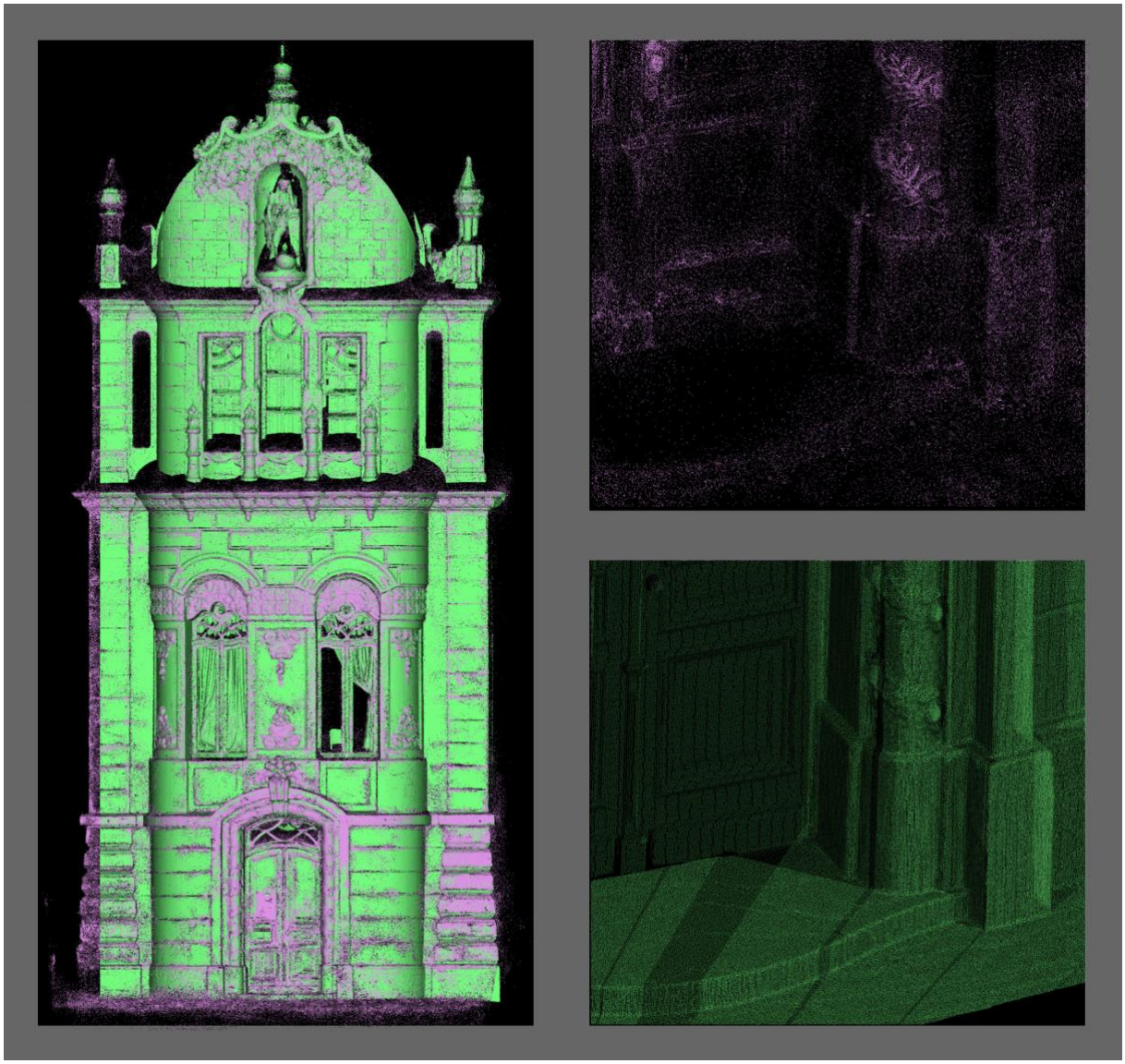


Figure 11: Comparison of the 3DGS (pink) and laser scanner (green) point clouds, overlapped on the left and isolated on the right.

CC BY

To align the models, a coarse-to-fine registration strategy was performed. Initial spatial alignment was established via the software's manual registration tool, which uses a three-point pair registration on distinct architectural features. Subsequently, the software's global registration tool was executed, which is based on the Iterative Closest Point (ICP) method. A sample size of 50,000 points was set (the maximum available setting) with a convergence tolerance set to zero. Convergence was achieved at 16 iterations, yielding an initial mean alignment distance of 21.6 mm with a standard deviation of 39.7 mm prior to spatial clipping.

Outliers were handled by establishing a maximum search distance threshold of 7 mm during the 3D comparison. Points exhibiting deviations beyond this limit (arising primarily from background noise, internal features captured through window glass, and the inherent 3DGS floating radiance artifacts) were classified as non-corresponding spatial outliers and excluded from the geometric error metrics. The sampling strategy for geometric verification utilized a nearest-neighbor point-to-point evaluation protocol within the software's 3D compare tool. Following outlier handling, a total dataset of 354,209 resulting corresponding points distributed across the main facade surface was evaluated to construct the error distribution.

Quantitative error analysis yielded a mean geometric deviation of 3.3 mm, a standard deviation of 3.9 mm, and an RMS error of 3.9 mm. As illustrated by the deviation spectrum and histogram (Figure 10), the absolute error distribution exhibits non-Gaussian asymmetry. Evaluating absolute error magnitudes, the median deviation (50th percentile) is located at 2.9 mm, while the 90th percentile threshold is bounded at 5.5 mm. The quality of the 3DGS cloud can be evaluated through the 3D deviation analysis illustrated in Figure 10. Additionally, the point clouds can be compared through their overlapped and isolated representations, with the scanner shown in green and the 3DGS in pink (Figure 11).

The comparison in Figure 12, which features the facade photo alongside renderings of the 3DGS and laser scanner models, reveals superior photorealism in the 3DGS model. This is particularly evident in the rendering of textures, reflections, and the transparency of the window glass. While the quality of both outputs declines toward the upper part of the facade due to the absence of aerial drone data, the 3DGS remains visually compelling.

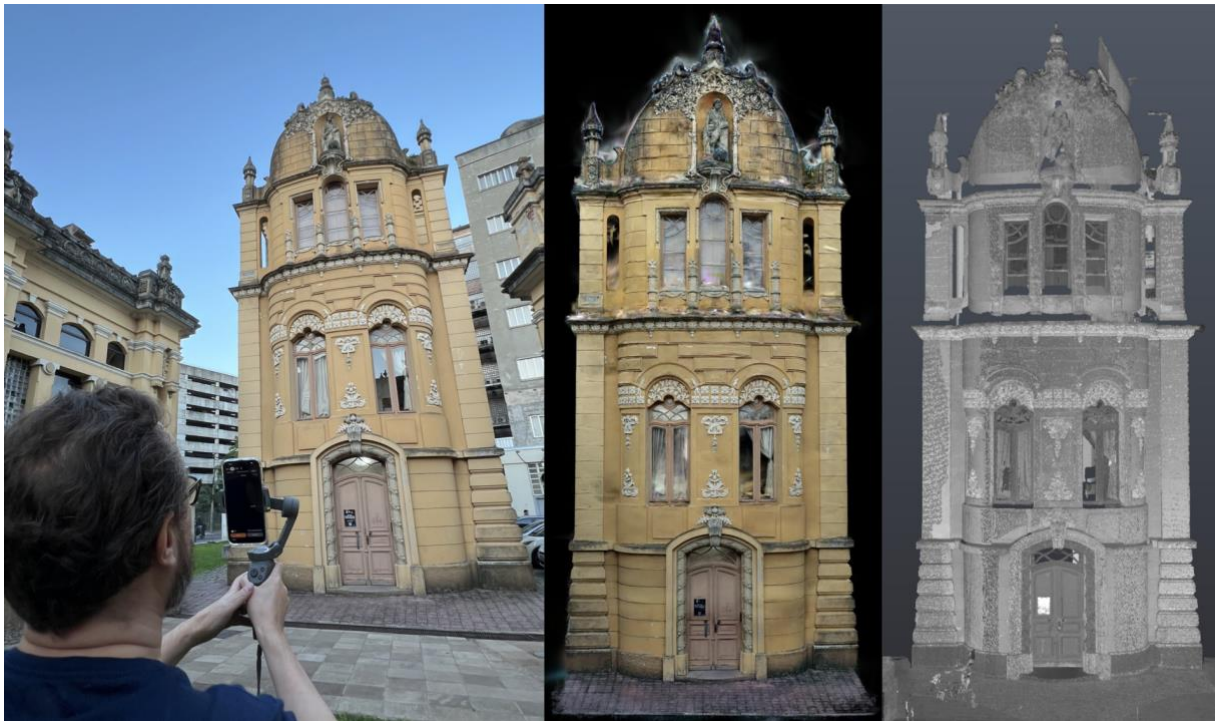


Figure 12: Comparison of the rendering of the 3DGS digitization (center) and the laser scanner (right) relative to the photo of the Observatory (left).

Based on the results obtained, it can be concluded that the 3DGS technique employed is not suitable for strict metrological purposes due to its lower geometric precision and susceptibility to floating radiance artifacts, which

demand explicit spatial filtering. The lack of an absolute coordinate system in native 3DGS and the absence of Ground Control Points (GCPs) during the purely visual capture could be addressed in future workflows to improve accuracy. However, 3DGS offers higher photorealism at a lower cost. The reality capture setup employed for 3DGS in this study (consumer smartphone, handheld gimbal, and open-source software pipelines) represents an initial field hardware investment below $1,500 USD. In contrast, high-end TLS systems typically require a capital expenditure around $60,000 USD. This represents a field acquisition hardware expenditure reduction exceeding 95%. While the total end-to-end workflow duration shows a modest overall difference (66.5 minutes for 3DGS versus 75 minutes for laser scanner), 3DGS achieves a major operational advantage in field capture efficiency, requiring only 8 minutes of total on-site acquisition compared to 55 minutes for TLS station setups and scanning. Conversely, 3DGS shifts the computational burden to the laboratory stage during neural optimization. Although these workflow metrics represent preliminary findings from a single campaign, they demonstrate that 3DGS is a compelling alternative for visual documentation, stakeholder communication, and rapid site surveys.

4.7 BIM-integrated navigation via a splat-plus-collider configuration

Maturity level: concept (application pattern; no implementation or measurement reported in this study).

BIM viewers such as Autodesk Viewer, Navisworks, or IFC.js expose structured semantic data but render a stylized representation that diverges from the as-built site (J. Zhu & Wu, 2022), whereas web-based point-cloud and mesh viewers such as Cesium 3D Tiles or Potree carry the as-built appearance but lack deep BIM-semantic linkage. The present use case addresses this gap through a fused architecture that pairs a photorealistic splat for the visual layer with an invisible BIM-derived collision mesh for all geometry operations, thereby combining the strengths of both. The underlying pattern, pairing invisible collision geometry with a separate visual representation, is long established in game engines and AEC co-visualization; the contribution of this work is its transfer to the splat register.

The configuration is realized in three layers (Figure 13). The visual layer is a 3DGS splat rendered by a tile-based WebGL rasterizer (Three.js `GLSplatMesh`, Babylon.js, or Cesium 3D Tiles); it is never raycasted against and remains purely presentational. The collision layer is an invisible mesh, derived either from BIM (IFC → IfcOpenShell → glTF / 3D Tiles) or from a coarse SfM/LiDAR reconstruction via Scan-to-BIM pipelines (Luo et al., 2026), against which all raycasting, measurement, and element tagging is executed. Finally, a semantic bridge in the form of a JSON sidecar links mesh face groups or GUIDs to BIM metadata and external databases (CAFM, sensor streams, inspection records), so that click events trigger a contextual metadata popup.

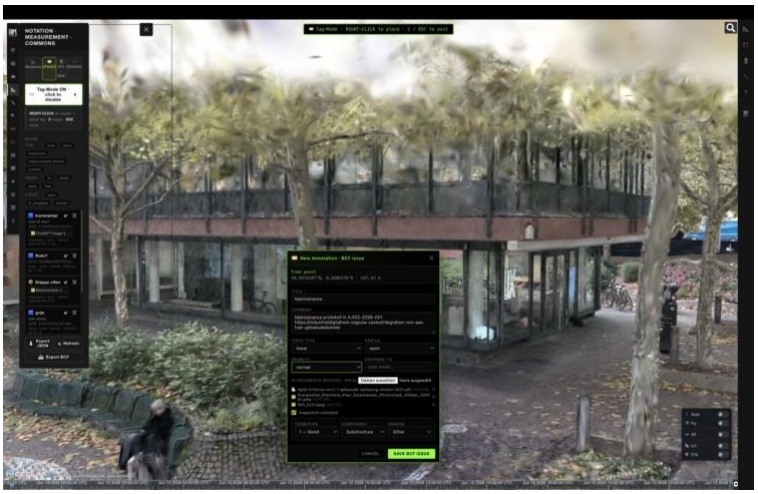


Figure 13: Splat-plus-collider navigation in a browser viewer, with a contextual annotation/metadata panel (right).

The collision mesh imposes negligible GPU overhead, and splat rendering holds real-time rates at 1080p on consumer GPUs (Kerbl et al., 2023), so the configuration supports low-latency navigation. Update cost remains low because only the splat, not the collision geometry, needs retraining when the as-built state changes. Integration effort, by contrast, is high: the value of the approach rests entirely on the quality of the mesh–BIM linkage and on

CC BY

a stable registration between the layers, the failure of which (registration drift, clicks hitting the wrong element) constitutes the principal risk. Metric accuracy is high only as inherited from the BIM/LiDAR mesh, since the splat itself contributes nothing measurable.

4.8 Superstructure inspection and damage classification

Maturity level: concept (acquisition and processing parameters specified; no quantitative results from an own campaign reported).

Bridges, tunnels, facade panels, and retaining walls require periodic inspection for cracks, spalling, delamination, and corrosion (Alfaro et al., 2025), yet physical access through scaffolding, rope-access, or lane closures is expensive, slow, and hazardous. Drone-based 2D imagery produces spatially disconnected photos that cannot directly support longitudinal crack-width measurement or structured annotation in a common coordinate system. 3DGS instead provides spatial continuity, colour fidelity, and zoomable detail, whereas metric crack-width estimation relies on the companion collision mesh.



Figure 14: 3DGS reconstruction of a derelict steel-frame industrial hall (Leimen, Germany), LiDAR/3DGS hybrid. The splat supports visual review; quantitative measurement is derived from the companion LiDAR mesh.

The acquisition follows a systematic nadir-and-oblique drone flight (DJI Matrice / Mavic 3 Enterprise) with more than 80 % front and more than 60 % side overlap, capturing facades at ≤5 cm GSD with onboard RTK or ground control points. Camera poses are then recovered and the splat is trained using COLMAP-PCD (Bai et al., 2024) with LiDAR bundle adjustment, with 3DGS training taking 30–90 min. Within the resulting inspection interface, per-cycle annotation layers (crack polygons, spalling, corrosion) are stored as GeoJSON against the collision-mesh frame and differenced between inspection cycles, while crack-width estimation is obtained by raycasting through opposing crack-wall picks on the collision mesh (LiDAR or high-accuracy MVS). Damage classification builds on CNN-based crack detectors applied to individual drone frames (Alfaro et al., 2025), which are registered into the 3DGS coordinate system to create a spatially anchored damage map; the splat thereby enables remote visual verification and context that 2D photo grids cannot provide (Figure 14).

On spatial continuity, colour fidelity, and remote reviewability, 3DGS supports visual inspection more effectively than disconnected 2D photo grids, with on-site effort typically a single campaign day. The metric limitation is decisive and stated as a hard constraint, not a caveat: the splat *cannot* provide sub-millimetre crack-width measurement, its centimetre-level error being one to two orders of magnitude coarser than the feature measured. Even with RTK/GCP control, the splat is a localization and visualization aid; *all* quantitative damage assessment must come from a LiDAR- or high-accuracy-MVS mesh. Hence metric accuracy rates “high” only with the qualifier “LiDAR mesh required”.

CC BY

4.9 Long-term documentation of listed structures

Maturity level: concept (workflow and archiving strategy proposed; no multi-epoch change-detection results reported).

Historic buildings, monuments, and listed structures (*Baudenkmäler*) require documentation serving three constituencies: preservation authorities (evidence-based assessment), architects and engineers (refurbishment planning), and craftspeople (execution reference) (Salah et al., 2025). No single modelling approach offers both geometric accuracy and visual fidelity, since laser scans capture geometry but not colour or patina, photography provides colour but no spatial context, and photogrammetric meshes are expensive to repeat annually. 3DGS is well suited to combine spatial completeness with photographic colour fidelity at comparatively low recurring cost (Figure 15).



Figure 15: 3DGS capture of a listed dry-stone masonry structure with vaulted openings. The splat preserves surface patina, vegetation, and colour; geometry for preservation decisions is taken from the companion LiDAR layer.

The workflow rests on repeat campaigns of one to two captures per year (drone and handheld) with consistent georeferencing via GCPs or RTK. Each epoch is archived as `.splat` / glTF (`KHR_gaussian_splatting`) in a versioned store (CDE, Nextcloud, NAS), with USD-based frameworks (Oh & Yu, 2025) structuring the time series. Change detection is performed through a voxel-wise diff between epochs that highlights volumetric change such as material loss, crack propagation, or biological growth, with thresholded change masks exported as annotated overlays. These annotation layers are connected to a CAFM or HBIM database (Yu et al., 2026) for maintenance linkage, with the 3DGS viewer serving as the spatial interface, while dissemination is handled through a public web viewer (60 fps, no plugin) and expert users retain access to the full-resolution archive.

Recurring on-site effort is low (a single campaign day, no scaffold for documentation), and the photorealistic record is remotely accessible to all stakeholders, which motivates the low update-cost and high visual-fidelity ratings. Two qualifications apply: first, geometry for preservation decisions should come from the LiDAR layer, not the splat, hence the medium metric rating (Yu et al., 2025); second, the open-format archiving argument is conditional, since `KHR_gaussian_splatting` was not yet ratified at the time of writing. Until then, long-term format stability rests on documented migration paths rather than a stable standard, which is the principal risk for this case.

4.10 Cross-case overview

The preceding cases differ substantially in acquisition setup, scale, evaluation depth, and maturity. To make the cross-case conclusions drawn in Section 5 traceable to the underlying evidence, Table 6 consolidates the key characteristics and reported metrics of all cases along the dimensions of the analytical framework. Cells marked "n.r." indicate that the respective figure was not reported in the underlying study; cells marked "n.a." indicate that the dimension does not apply to the case. The comparatively large number of n.r. entries is itself a finding: reporting practice in this field is not yet standardised, which is one of the motivations for the minimal evaluation set proposed in Section 6.2.

CC BY

Table 6: Cross-case evidence overview.

Case	Maturity level	Sensor / input data	Scene scale	Baseline / reference	Acquisition time	Training / processing time	Hardware (GPU, CPU, RAM)	Model size / no. of Gaussians
4.1 Synthetic training data for damage segmentation	Concept	Photogrammetric imagery with oriented images + classified 3D point cloud	n.r.	Qualitative comparison only (game-engine rendering, NeRF, direct label projection); no quantitative baseline	n.r.	n.r.	n.r.	n.r.
4.2 Construction-site documentation in VR	Experimentally validated (beam, room); implemented prototype (4 site scenarios)	Smartphone video, ultra-wide lens, 4K @ 60 fps	Beam 8.847 × 0.956 × 0.769 m; room 15.84-16.71 × 2.005-3.835 × 2.800 m; shell apartment, reinforcement cage, TBE detail + room	TLS (beam, room); MLS; photogrammetry; LiDAR; no reference for the 4 site scenarios	n.r.	30-90 min (Kerbl et al. implementation); 30–60 min (Polycam), 2024 campaign	"Powerful graphics hardware" required; specification n.r.	n.r.; large data volume reported as main limitation
4.3 3DGS-to-IFC conversion	Implemented prototype	Point cloud derived from a 3DGS indoor reconstruction	Single room	5 automated segmentation methods evaluated (SOR/ROR, region growing, distance/density clustering, plane detection, PointNet++ on S3DIS) – all rejected as unreliable; no geometric reference	n.r.	≈ 1 h per room, of which ≈ 80 % manual segmentation	n.r.	2.6 M raw → 1.6 M cleaned → 1.3 M in 15 segments → 2.65 M after 10 mm infill → 69.7 K after 50 mm voxel grid; mesh 230 vertices / 400 triangles
4.5 Concrete condition assessment for circular reuse	Implemented prototype	Video sequences + targeted detail image sets	Dismantled cast-in-place elements, university building (RUB)	*Literature comparison 3DGS vs. laser scanning (Hagedorn et al., 2026)*; no own quantitative baseline	n.r.	30 k training steps; wall-clock time n.r.	n.r.	Postshot by Jawset v0.6.150, Splat3 profile, max. 3,000 k splats, anti-aliasing enabled
4.6 Astronomical observatory facade	Experimentally validated	iPhone 15 Pro Max + DJI Osmo Mobile 3 gimbal, SplatKing app, fixed ISO/shutter/WB; 462 photos (231 @ 25 mm, 231 @ 14 mm)	Main facade, listed building (1908)	Z+F Imager 5010C TLS, 3 scan positions, 14.6 M pts; nominal 0.4 mm RMS @ 10 m, linear accuracy ≤ 1 mm	8 min (3DGS) vs. 45 min scanning + 10 min setup (TLS)	3.5 min alignment (RealityScan v2.1.1) + 55 min training (LichtFeld Studio v0.5.1) = 66.5 min total; TLS 20 min (Recap 2026) = 75 min total	Intel i9-13900F, 128 GB RAM, RTX 4070 (12 GB VRAM); identical workstation for both methods	3 M Gaussians, SH degree 3; derived point cloud 2 M pts

CC BY

Case	Maturity level	Sensor / input data	Scene scale	Baseline / reference	Acquisition time	Training / processing time	Hardware (GPU, CPU, RAM)	Model size / no. of Gaussians
4.7 BIM-integrated navigation (splat + collider)	Concept	3DGS splat (visual layer) + BIM-derived collision mesh (IFC → IfcOpenShell → glTF / 3D Tiles) or coarse SfM/LiDAR mesh + JSON sidecar	n.r.	Qualitative comparison against BIM viewers (Autodesk Viewer, Navisworks, IFC.js) and point-cloud viewers (Cesium 3D Tiles, Potree)	n.r.	n.r.; only the splat requires retraining on as-built change	Consumer GPU assumed; specification n.r.	n.r.
4.8 Superstructure inspection and damage classification	Concept	DJI Matrice / Mavic 3 Enterprise, nadir + oblique flight, > 80 % front / > 60 % side overlap, ≤ 5 cm GSD, RTK or GCP; LiDAR/3DGS hybrid	Bridges, tunnels, facade panels, retaining walls; example: derelict steel-frame industrial hall, Leimen (DE)	LiDAR mesh or high-accuracy MVS; 2D drone photo grids	Single campaign day	COLMAP-PCD with LiDAR bundle adjustment; 3DGS training 30–90 min	n.r.	n.r.
4.9 Long-term documentation of listed structures	Concept	Drone + handheld capture, GCP/RTK georeferencing; 1–2 campaigns per year	Historic buildings, monuments, listed structures; example: dry-stone masonry with vaulted openings	LiDAR layer as geometric reference; annual photogrammetric meshes as cost baseline	Single campaign day, no scaffolding	n.r.	n.r.	Archived as .splat / glTF (*KHR_gaussian_splatting*, not yet ratified); versioned store (CDE, Nextcloud, NAS), USD-structured time series

n.r. = not reported in the underlying study; n.a. = not applicable to this case. Values in *italics* are cited from the literature or stated as target values and were not measured within this study.

5. DISCUSSION

5.1 Positioning 3DGS within the reality capture landscape

The results across the investigated use cases demonstrate that 3DGS occupies a unique position within the landscape of reality-capturing technologies. Unlike established sensing technologies such as TLS, LiDAR, or photogrammetry, 3DGS is not primarily designed to generate metrically accurate geometric representations. Instead, it focuses on the efficient generation of highly realistic and interactive scene representations from image-based data. Similar trade-offs between geometric accuracy and operational efficiency have previously been reported for photogrammetry-based approaches and mobile reality-capturing systems (Z. Chen et al., 2022; Sestras et al., 2025; R. Yu et al., 2022). The findings of this study suggest that 3DGS extends this development by prioritizing photorealistic scene representation and interactive visualization while maintaining comparatively low acquisition requirements.

This observation supports recent discussions in the reality-capturing literature that emphasize the growing importance of accessible and scalable data acquisition technologies for lifecycle-oriented building management and digital-twin development (Attaran & Celik, 2023; Hakimi et al., 2024). As the AECO sector increasingly relies on continuously updated digital representations of physical assets, the balance between geometric precision, acquisition effort, and usability becomes a critical consideration.

The findings indicate that 3DGS should therefore not be interpreted as a direct replacement for existing surveying and documentation methods. Rather, it represents a complementary paradigm that emphasizes visual realism,

CC BY

accessibility, and real-time rendering capabilities. Across multiple cases, including construction site documentation, heritage digitization, and facility-related applications, 3DGS consistently produced visually rich reconstructions while requiring comparatively low-cost acquisition equipment, such as consumer-grade smartphones and cameras.

This observation aligns with recent developments in radiance field rendering research, where the focus increasingly shifts from pure geometric reconstruction towards immersive and interactive scene representations. While laser scanning remains the preferred solution for applications requiring millimeter-level accuracy, such as deformation monitoring, dimensional verification, or engineering-grade surveying, 3DGS appears particularly suitable for applications where visual understanding, communication, and rapid documentation are of primary importance.

The comparison of the presented cases further reveals a fundamental trade-off between geometric accuracy and visual fidelity. For example, the cultural heritage case demonstrated that laser scanning achieved superior geometric precision, whereas 3DGS delivered substantially higher photorealism, particularly in representing reflective surfaces, transparency effects, and complex material appearances. Similar observations were made in the construction site documentation use case, where 3DGS provided a significantly more realistic perception of construction progress and spatial conditions than conventional point cloud representations.

Consequently, the results suggest that the future role of 3DGS within the AECO sector is likely to emerge not as a competing technology to established reality-capturing methods, but as an additional representation layer that complements existing workflows. In this context, 3DGS bridges the gap between reality capture and immersive digital-twin visualization by providing realism and accessibility that traditional point-cloud-based approaches struggle to achieve.

From a theoretical perspective, 3DGS may therefore be interpreted as a shift from geometry-centric reality capture towards perception-centric digital representations. This development aligns with recent discussions on human-centered digital twins, where visual understanding and contextual awareness are increasingly considered important complements to geometric accuracy (Cooperman & Bartels, 2026; Hakimi et al., 2024).

5.2 Cost and effort considerations

Cost is one of the recurring arguments for 3DGS in the reviewed literature, but it is rarely quantified. Table 6 therefore consolidates the cost and effort factors observed across the cases of this study and contrasts them with photogrammetry and TLS/LiDAR. The figures are indicative rather than normative: they originate from single campaigns under specific conditions (Sections 4.2, 4.3, 4.6, 4.8) and scale with project size, required accuracy, and the degree of manual post-processing.

The pattern across the cases is consistent: 3DGS shifts cost from capital expenditure and on-site time towards GPU compute and manual post-processing. It is therefore most advantageous where site access is expensive or constrained, where acquisition must be repeated frequently, and where no hardware investment can be justified – and least advantageous where a single, accuracy-critical campaign is required and a TLS is already available.

5.3 Applicability of 3DGS across AECO Domain

The diversity of the investigated use cases demonstrates that 3DGS can support a broad spectrum of AECO-related applications. Despite the methodological differences between the cases, several recurring patterns emerged regarding the types of scenarios that benefit most from the technology.

The broad applicability observed across the investigated cases reflects a wider trend within construction digitalization, where reality-capturing technologies are increasingly used not only for documentation but also for inspection, progress monitoring, facility management, and decision support (Anwar & Azhar, 2025; Salman & Ahmad, 2023)

A first group of applications relates to documentation and visualization. The construction site and cultural heritage cases showed that 3DGS enables the creation of highly realistic digital representations that facilitate remote inspections, stakeholder communication, training, and archival documentation. In these scenarios, the ability to intuitively understand spatial conditions often outweighs the need for engineering-grade geometric accuracy.

CC BY

Table 7: Cost and effort factors of 3DGS compared with photogrammetry and TLS/LiDAR.

Cost factor	3DGS	Photogrammetry	TLS / LiDAR
Field hardware (CAPEX)	< 1,500 USD: consumer smartphone, handheld gimbal, open-source pipeline (Section 4.6). Drone-based variants add a Mavic 3 Enterprise / Matrice class UAV (Sections 4.8, 4.9).	Comparable to 3DGS – identical image-based acquisition with standard cameras or drones (Section 2.2); no additional field hardware.	≈ 60,000 USD for a high-end TLS (Z+F Imager 5010C, Section 4.6). Field hardware expenditure for 3DGS is therefore more than 95 % lower.
Software / licences	Open-source or low-cost cloud services: reference implementation of Kerbl et al., Postshot by Jawset, Polycam, KIRI Engine, LichtFeld Studio, SuperSplat. All software used in Section 4.6 is free for academic purposes.	Mix of commercial SfM/MVS suites and open-source alternatives; RealityScan v2.1.1 was used for image alignment in Section 4.6.	Vendor processing software, typically licensed per seat; Autodesk ReCap 2026 in Section 4.6.
Compute hardware	Dedicated GPU required: RTX 4070 (12 GB VRAM), Intel i9-13900F, 128 GB RAM (Section 4.6). High-quality models are explicitly reported as demanding powerful graphics hardware (Section 4.2).	GPU beneficial but with lower VRAM demand; outputs are substantially smaller (Section 4.2).	Standard workstation sufficient; the same machine processed both pipelines in Section 4.6.
On-site acquisition time	8 min for 462 images of the observatory facade (Section 4.6); one campaign day for drone-based superstructure and heritage capture (Sections 4.8, 4.9).	Comparable to 3DGS, since acquisition is identical; not reported separately in this study.	55 min for the same facade: 45 min scanning across three stations plus 10 min setup (Section 4.6).
Operator skill level	Low for acquisition (locked exposure, smooth camera motion, sufficient overlap); high for training, artifact filtering, scaling, and post-processing.	Low for acquisition; moderate for processing and quality control.	High throughout: station planning, registration, and georeferencing require surveying expertise.
Training / processing time	3.5 min alignment + 55 min training (Section 4.6); 30-90 min for the reference implementation and 30-60 min for Polycam (Section 4.2); 30-90 min for the drone-based case (Section 4.8).	Not reported separately; the Polycam photogrammetry output in Section 4.2 produced markedly smaller and simpler models.	20 min in Autodesk ReCap 2026 (Section 4.6).
Manual post-processing to BIM	≈ 1 h per room, of which ≈ 80 % is manual segmentation; all five automated segmentation methods tested proved unreliable on 3DGS-derived data (Section 4.3).	Not reported in this study.	Not reported in this study; established Scan-to-BIM workflows reach higher levels of development than the LOD 200 achieved from 3DGS (Section 6).
Total end-to-end duration	66.5 min (Section 4.6).	Not reported in this study.	75 min (Section 4.6). The difference in the total is modest; the advantage of 3DGS lies in how the effort is distributed, not in the sum.
Data volume and storage	High; explicitly named as a main limitation (Section 4.2). Each documentation epoch is archived as .splat / glTF (Section 4.9).	Substantially smaller file sizes and simpler models, at the cost of missing detail and artifacts (Section 4.2).	14.6 M points for a single facade, against 2 M points in the cloud derived from the 3DGS model (Section 4.6).
Cost per repeat epoch	Low: acquisition only. The collision geometry is reused and only the splat is retrained when the as-built state changes (Sections 4.7, 4.9); one to two campaigns per year are considered feasible (Section 4.9).	Photogrammetric meshes are described as expensive to repeat annually (Section 4.9).	High: the full station setup and registration effort recurs with every epoch.

All figures are indicative, not normative. They originate from single campaigns under specific conditions (Sections 4.2, 4.3, 4.6, 4.8) and scale with project size, required accuracy, and the degree of manual post-processing. Section references point to the case from which the respective figure is taken.

A second group comprises inspection and assessment applications. The condition assessment of concrete elements and damage documentation workflows illustrate how 3DGS can serve as a visually rich foundation for integrating

CC BY

automated analysis methods. In these cases, the scene representation functions as a contextual layer that supports the localization and interpretation of detected defects while maintaining a close connection to the original physical environment.

A third and particularly promising application area concerns the integration of artificial intelligence. The semantic segmentation use case highlights the potential of 3DGS as a tool for generating synthetic training data with a comparatively small domain gap. Unlike conventional synthetic environments generated in game engines, 3DGS-based datasets preserve the visual characteristics of real-world environments while enabling the efficient creation of new viewpoints and automatically labeled data. This capability may significantly reduce the effort required for dataset generation and improve the robustness of machine-learning models in construction-specific applications. The ability to generate realistic synthetic training data is particularly relevant in construction, where annotated datasets remain scarce and expensive to produce. Previous studies have identified limited availability of training data as a major barrier to the adoption of machine-learning approaches in defect detection, progress monitoring, and automated quality assurance (Oytun & Atasoy, 2022; Pan et al., 2022; Zahs et al., 2023).

Taken together, the cases indicate that the greatest benefits of 3DGS are realized in applications that prioritize visual information, contextual understanding, and interaction rather than highly precise geometric measurements. This suggests that future adoption within the AECO sector may initially be driven by visualization, communication, inspection, and AI-supported workflows before expanding into more geometry-centric applications.

Consequently, 3DGS may contribute to overcoming one of the persistent challenges of construction digitalization: the efficient generation of high-quality visual information that can simultaneously support human decision-making and machine-learning applications.

5.4 Towards intelligent digital twins: Integrating 3DGS into BIM and AI workflows – potentials and open gaps

One of the most significant findings emerging from the cross-case analysis is that the value of 3D Gaussian Splatting extends beyond photorealistic visualization. While the technology is often discussed primarily as a radiance field rendering approach, the investigated use cases demonstrate its potential to act as an intermediary layer between reality capture, digital-twin environments, BIM, and AI-driven analysis workflows. Digital twins are commonly understood as dynamic digital representations that continuously integrate information from physical assets throughout their lifecycle (Attaran & Celik, 2023). Despite significant progress in BIM and sensing technologies, many digital twins in the built environment remain limited by incomplete as-built information, infrequent updates, and costly data acquisition processes (Cooperman & Bartels, 2026; Hakimi et al., 2024).

Traditionally, reality-capturing processes in the AECO sector follow a geometry-centered paradigm. Data acquisition technologies such as laser scanning, LiDAR, or photogrammetry generate point clouds or meshes that subsequently serve as the basis for Scan-to-BIM workflows and digital-twin development. Although these approaches provide accurate geometric representations, they often require extensive post-processing, manual modeling, and significant expert knowledge before the captured data can be integrated into operational workflows.

The presented cases suggest that 3DGS introduces an alternative perspective. Instead of focusing exclusively on geometric reconstruction, 3DGS generates highly realistic scene representations that preserve visual information, contextual relationships, and environmental conditions. This creates a digital representation that is closer to human perception and therefore particularly valuable for inspection, communication, training, and decision-support applications.

The BIM integration use case demonstrates that 3DGS models can be systematically transformed into BIM-compatible representations through point-cloud extraction, geometric abstraction, and IFC generation. Although this workflow currently requires several intermediate processing steps, it illustrates the feasibility of linking volumetric scene representations with established BIM standards. In this regard, 3DGS may be viewed as an additional layer within future Scan-to-BIM pipelines rather than a replacement for existing approaches. The technology simplifies data acquisition while maintaining sufficient information richness to support subsequent semantic modeling processes. These findings correspond with ongoing research efforts aiming to bridge the gap between reality-capturing technologies and BIM environments through automated Scan-to-BIM workflows (Gumowski, 2025; Xing et al., 2025). While laser scanning and photogrammetry currently dominate this field,

CC BY

3DGS introduces an alternative pathway that combines low-cost data acquisition with highly realistic scene representations.

A particularly promising finding concerns the relationship between 3DGS and artificial intelligence. Several use cases illustrate how 3DGS scene representations can facilitate AI-supported workflows. The semantic segmentation case demonstrates the generation of large-scale synthetic training datasets through automatic view synthesis and label transfer. Unlike conventional synthetic environments created in game engines, 3DGS preserves the visual characteristics of real-world construction environments, thereby reducing the domain gap that frequently limits the applicability of machine-learning models. Similarly, the concrete condition assessment case combines 3DGS with automated damage detection and semantic enrichment processes, enabling the integration of visual inspections, defect localization, and BIM-based inventory generation. The integration of AI and digital twins is increasingly recognized as a key component of Construction 4.0 and intelligent asset management (Ghansah, 2024). In this context, 3DGS offers a unique advantage by providing both visual context and scalable data generation capabilities, thereby creating new opportunities for AI-supported inspection, monitoring, and predictive maintenance.

These findings indicate that 3DGS may evolve into an enabling technology for AI-driven digital twins. Rather than serving merely as a visualization component, the technology provides a rich spatial context in which machine-learning algorithms can operate, generate annotations, identify defects, and support decision-making processes. In this sense, 3DGS functions not only as a representation of reality but also as a data environment that connects physical assets with intelligent analytical processes. This potential should, however, be calibrated against what the cases actually demonstrate. All cases operate on discrete, manually triggered capture campaigns. None of them demonstrates continuous synchronisation between the physical asset and its representation, none maintains a persistent state that is updated rather than replaced, none couples the representation to operational data such as sensor streams, BMS data, or maintenance records at runtime, and none closes a feedback loop from the representation back to a decision or actuation on the asset. The repeat-campaign workflow in Section 4.9 is the closest approximation, but it is a concept operating at an annual to semi-annual interval and has not yet been executed across multiple epochs. What the cases support is therefore the narrower claim that 3DGS is a promising visualisation and integration layer for digital twins; the step from this layer to a continuously updated digital twin remains to be demonstrated.

From a digital-twin perspective, this development is particularly relevant. Current digital twins in construction and facility management often suffer from incomplete, outdated, or costly-to-maintain representations of the physical asset. The low-cost acquisition and comparatively rapid generation of 3DGS models may enable more frequent updates of digital representations throughout the building lifecycle. Consequently, 3DGS could in principle support a shift from static digital models towards more frequently updated digital representations. Whether this translates into continuously evolving digital twins depends on capabilities that lie outside the scope of the present cases – automated triggering of re-capture, incremental rather than full re-training, and persistent linkage of successive epochs to a common semantic state – and remains an open research question.

Overall, the results suggest that the long-term significance of 3DGS for the AECO sector may not primarily lie in replacing existing reality-capturing technologies. Instead, its contribution appears to reside in establishing a new integration layer between reality capture, semantic building information, and artificial intelligence. Should the synchronisation and state-persistence gaps identified above be closed, such a role would position 3DGS as an enabler for the next generation of intelligent and continuously updated digital twins. On the evidence presented here, this remains an outlook rather than a demonstrated outcome.

6. CONCLUSION AND FURTHER RESEARCH

This paper examined the fundamentals and applications of 3D Gaussian Splatting (3DGS) in the AECO sector by combining a systematic literature review with a multiple-case study and a dedicated 3DGS-to-IFC conversion pipeline. With respect to the first research question, we have demonstrated that the scenarios benefiting most from 3DGS are those in which visual realism, contextual understanding, and interaction outweigh the need for millimetre-level geometric accuracy: construction-site documentation and progress communication, remote and preliminary inspection, cultural-heritage digitisation, and – most distinctively – the generation of realistic, automatically labelled synthetic training data for machine learning.

CC BY

Regarding the second research question, the cases demonstrate that 3DGS integrates into existing capturing workflows through low-cost image- or video-based acquisition and real-time rendering; the 3DGS-to-IFC pipeline confirms the feasibility of feeding volumetric scene representations into BIM environments (at approximately LOD 200), positioning 3DGS as an additional layer within Scan-to-BIM rather than as a substitute for it. This integration, however, involves clear trade-offs: gains in on-site acquisition time, hardware cost, and real-time rendering are offset by a shift of effort towards GPU training and manual post-processing (Table 6), as well as by limited geometric accuracy and the absence of a native metric scale, large data volumes and GPU demand (Section 4.2), and a resulting cap at approximately LOD 200 in the IFC conversion, rather than the higher-precision levels achievable with TLS-based Scan-to-BIM.

Concerning the third research question, the principal challenges are the limited geometric precision and the absence of an absolute scale in native 3DGS, the large data volume and GPU demand of high-quality models, the dependence on training, and the current lack of standardised evaluation metrics. We propose that these can be mitigated through hybrid acquisition (e.g. TLS-initialised or ground-control-point-referenced 3DGS) and surface-oriented variants, though this remains to be validated in future work.

Across all cases, we have shown that 3DGS emerges not as a competitor to established surveying technologies but as a complementary, perception-centric representation layer. We hypothesise that its longer-term contribution could lie in bridging reality capture, semantic building information, and artificial intelligence. Realising potentially continuously updated, intelligent digital twins on this basis would additionally require continuous synchronisation, persistent state updates, coupling to operational data, and a closed feedback loop – none of which is demonstrated by the cases presented here.

6.1 Limitations

The findings are subject to several limitations. The heterogeneity of the cases and the absence of standardised 3DGS evaluation metrics for AECO contexts restrict direct quantitative comparison. As an emerging technology, 3DGS is still predominantly applied in research rather than routine practice, so the cases reflect exploratory rather than fully matured workflows. The case selection is further constrained geographically and institutionally, with a strong representation of the German-speaking research context, which may limit generalisability. Finally, native 3DGS lacks an absolute coordinate system, and high-fidelity models remain demanding in terms of data volume and graphics hardware. Taken together, these limitations mean that the present findings demonstrate feasibility and current performance under exploratory conditions, rather than validated performance in routine, long-term AECO practice.

Evaluation practice across the reviewed studies varies considerably, ranging from qualitative visual inspection to point-cloud-based distance metrics (e.g. cloud-to-cloud, C2C) against TLS or MLS references, dimensional spot-checks of individual building elements, and subjective quality/usability ratings, with no consistent set of metrics applied across studies or scenarios. This heterogeneity limits the comparability of results reported in Section 4 and underlines the need for a standardised evaluation framework, discussed further in Section 6.2.

6.2 Outlook and further research

Future work should advance 3DGS along four directions. The following therefore represent proposed research directions and anticipated potential rather than demonstrated outcomes of the present study. First, metric reliability: geo-referencing, ground control points, TLS-initialised training, and surface-oriented formulations (e.g. 2DGS, SuGaR) to close the precision gap for measurement-critical tasks. Closing this gap also requires establishing standardised evaluation metrics for 3DGS in AECO contexts, as no common benchmark currently exists. Building on the metrics used across the reviewed studies, a minimal evaluation set could combine: (i) geometric accuracy metrics such as cloud-to-cloud (C2C) distance against a TLS or MLS reference, reported as mean/standard deviation and normalized against the relevant object or room dimension to account for scale-dependence; (ii) direct dimensional checks of selected macroscopic features (e.g. wall length, element spacing) as a complementary, application-relevant accuracy indicator; (iii) visual/perceptual quality metrics (e.g. PSNR, SSIM, LPIPS) commonly used in the 3DGS literature but rarely reported in AECO-specific studies; (iv) practical performance indicators such as processing time, file size, and rendering frame rate, relevant for on-site and mobile deployment; and (v) task-based usability ratings (e.g. Likert-scale assessments of detail recognizability or viewer usability) to capture user-perceived quality beyond purely geometric measures. Adopting such a combined metric set in future

CC BY

studies would enable direct, cross-study comparison of 3DGS performance and its trade-offs against established surveying technologies. Second, interoperability: more automated and higher-LOD 3DGS-to-BIM/IFC workflows that preserve semantic and condition information. Third, intelligence: exploiting 3DGS as a scalable data environment for AI – synthetic training-data generation, defect detection, and semantic segmentation – as well as temporal (4D) 3DGS for construction-progress and longitudinal condition monitoring. Fourth, validation and deployment: broader, real-world, multi-region case studies, together with compression and streaming techniques that enable mobile and web-based use. Pursuing these directions would help 3DGS evolve from a visualisation tool into a core enabler of continuously updated, AI-driven digital twins across the building lifecycle. A fifth direction follows directly from the digital-twin gap identified in Section 5.4. Substantiating the digital-twin claim requires evidence on four specific capabilities: continuous or event-triggered synchronisation between asset and representation; persistent state updates in which successive epochs update rather than replace a common semantic state; runtime coupling to operational data such as sensor streams, BMS data, or maintenance records; and a closed feedback loop in which observations derived from the representation demonstrably inform decisions or actions on the asset. Longitudinal multi-epoch studies reporting these four capabilities would be required before 3DGS can be described as a core enabler of continuously updated, AI-driven digital twins across the building lifecycle, rather than as a visualisation and integration layer for them.

REFERENCES

Al Shafian, S., Xu, H., Khalid, A., & Hu, D. (2025). Simulating Real-World Damage Environments for Interactive Virtual Reality Training via 3D Gaussian Splatting. 2025 IEEE 4th International Conference on Intelligent Reality (ICIR), 1–4. https://doi.org/10.1109/ICIR68135.2025.11361594

Alfaro, M. C., Vidal, R. S., Delgadillo, R. M., Moya, L., & Casas, J. R. (2025). Structural damage detection using an unmanned aerial vehicle-based 3D model and deep learning on a reinforced concrete arch bridge. Infrastructures, 10(2), 33. https://doi.org/10.3390/infrastructures10020033

Anwar, R. M. I., & Azhar, S. (2025). A systematic review on the application of reality capture in the construction industry. Smart and Sustainable Built Environment. https://doi.org/10.1108/SASBE-03-2024-0079

Apffel, A., Tran, H., & Chheang, V. (2026). Nevis Digital Twin: Photogrammetry and Immersive Visualization of Historical Sites. 2026 IEEE Conference on Virtual Reality and 3D User Interfaces Abstracts and Workshops (VRW), 5–9. https://doi.org/10.1109/VRW70859.2026.00008

Attaran, M., & Celik, B. G. (2023). Digital twin: Benefits, use cases, challenges, and opportunities. Decision Analytics Journal, 6, 100165. https://doi.org/10.1016/j.dajour.2023.100165

Bai, C., Fu, R., & Gao, X. (2024). Colmap-PCD: An open-source tool for fine image-to-point cloud registration. 2024 IEEE International Conference on Robotics and Automation (ICRA), 1723–1729. https://doi.org/10.1109/ICRA57147.2024.10611582

Barsanti, S. G., & Elefante, E. (2026). Challenges and Capabilities of 3DGS in Detecting Tiny Details for Cultural Heritage. International Archives of the Photogrammetry, Remote Sensing and Spatial Information Sciences - ISPRS Archives, 48, 183–189. https://doi.org/10.5194/isprs-archives-XLVIII-2-W12-2026-183-2026

Bartels, N., Fuhrmann, A., Zou, Y., Würstlin, R. & Rittmeier, L. (2026). Smartphone-Based 3D Reconstruction of Buildings Using 3D Gaussian Splatting. Proceedings of the 43rd International CIB W78 Conference in New Delhi.

Basso, A., Condorelli, F., Giordano, A., Morena, S., & Perticarini, M. (2024). Evolution of rendering based on radiance fields: The Palermo case study for a comparison between NeRF and Gaussian Splatting. International Archives of the Photogrammetry, Remote Sensing and Spatial Information Sciences, XLVIII-2/W4-2024, 57–64. https://doi.org/10.5194/isprs-archives-XLVIII-2-W4-2024-57-2024

Botsch, M., Hornung, A., Zwicker, M., & Kobbelt, L. (2005). High-quality surface splatting on today's GPUs. Proceedings of the Eurographics Symposium on Point-Based Graphics 2005, 17–24.

Botsch, M., & Kobbelt, L. (2003). High-quality point-based rendering on modern GPUs. 11th Pacific Conference onComputer Graphics and Applications, 2003. Proceedings., 335–343. https://doi.org/10.1109/PCCGA.2003.1238275

Cai, Z., Yang, J., Wang, T., Huang, H., & Guo, Y. (2024). 3D reconstruction of buildings based on 3D Gaussian splatting. International Archives of the Photogrammetry, Remote Sensing and Spatial Information Sciences, XLVIII-4/W10-2024, 37–43. https://doi.org/10.5194/isprs-archives-XLVIII-4-W10-2024-37-2024

Carmeliti, M., & Marziali, S. (2026). A comparative evaluation of 3D reconstruction with photogrammetry, NeRFs and 3D Gaussian Splatting in Cultura Heritage Restoration. International Archives of the Photogrammetry, Remote Sensing and Spatial Information Sciences - ISPRS Archives, 48, 89–96. https://doi.org/10.5194/isprs-archives-XLVIII-2-W12-2026-89-2026

Çelik, F., Herbers, P., & König, M. (2024). Image Segmentation on Concrete Damage for Augmented Reality Supported Inspection Tasks. In S. Skatulla & H. Beushausen (Eds.), Advances in Information Technology in Civil and Building Engineering (Vol. 357, pp. 237–252). Springer International Publishing. https://doi.org/10.1007/978-3-031-35399-4_19

Chai, P., Hou, L., Lo, X., Zhang, G., Chen, H., & Zou, Y. (2025). Revolutionising construction site simulations with automated 3D segmentation and mesh construction. Smart Construction, 2(3). https://doi.org/10.55092/sc20250019

Chen, D., & Ma, J. (2026). Immersive VR visualization of urban building explosion accident consequences. Journal of Safety and Environment, 26(2), 438–445. https://doi.org/10.13637/j.issn.1009-6094.2025.1058

Chen, G., & Wang, W. (2025). A survey on 3D gaussian splatting. https://arxiv.org/abs/2401.03890

Chen, Z., Zhang, W., Huang, R., Dong, Z., Chen, C., Jiang, L., & Wang, H. (2022). 3D model-based terrestrial laser scanning (TLS) observation network planning for large-scale building facades. Automation in Construction, 144, 104594. https://doi.org/10.1016/j.autcon.2022.104594

Chiappini, S., Marcheggiani, E., Pierdicca, R., & Choudhury, M. A. (2025). Assessment of 3D Models of Rural Buildings Using UAV Images: A Comparison of NeRF, GS and MVS-SFM Methods. Lecture Notes in Civil Engineering, 586 LNCE, 1190–1197. https://doi.org/10.1007/978-3-031-84212-2_146

Chowdhury, S. D., Adesanya, M. A., Mohammed, N. A. C., &... (2026). Video-driven Gaussian splatting for as-built building geometry with energy simulation. … in Construction. https://www.sciencedirect.com/science/article/pii/S0926580526002220

Clini, P., Angeloni, R., D'Alessio, M., Coppetta, L., & Galli, I. (2025). Digital Representation and AI-driven Virtual Experience for Historic Houses. The Case Study of Borgo Storico Seghetti Panichi. International Archives of the Photogrammetry, Remote Sensing and Spatial Information Sciences - ISPRS Archives, 48, 337–344. https://doi.org/10.5194/isprs-archives-XLVIII-M-9-2025-337-2025

Clini, P., Nespeca, R., Angeloni, R., & Coppetta, L. (2024). 3D representation of architectural heritage: A comparative analysis of NeRF, Gaussian Splatting, and SfM-MVS reconstructions using low-cost sensors. International Archives of the Photogrammetry, Remote Sensing and Spatial Information Sciences, XLVIII-2/W8-2024, 93–99. https://doi.org/10.5194/isprs-archives-XLVIII-2-W8-2024-93-2024

Comte, F., Pamart, A., Réby, K., & De Luca, L. (2024). Strategies and experiments for massive 3d digitalization of the remains after the notre dame de paris fire. International Archives of the Photogrammetry, Remote Sensing and Spatial Information Sciences - ISPRS Archives, 48, 127–134. https://doi.org/10.5194/isprs-Archives-XLVIII-2-W4-2024-127-2024

Cooperman, A., & Bartels, N. (2026). Organizational framework for facility management information definition and delivery process. In Computing in civil engineering 2025 (pp. 620–630). https://doi.org/10.1061/9780784486436.066

Costantino, D., Vozza, G., Pepe, M., & Alfio, V. S. (2022). Smartphone LiDAR technologies for surveying and reality modelling in urban scenarios: Evaluation methods, performance and challenges. Applied System Innovation, 5(4). https://doi.org/10.3390/asi5040063

Dai, Y., Wu, J., & Wang, D. (2023). A review of common techniques for visual simultaneous localization and mapping. Journal of Robotics, 2023(1), 8872822. https://doi.org/10.1155/2023/8872822

Delgado-Martos, E., Montas-Laracuente, N., Pesqueira-Calvo, C., Intra Sidola, G., Maitín, A., Nogales, A., & García-Tejedor, Á. J. (2026). ARCHER: An integrated approach to artificial intelligence in the virtual

reconstruction of architectural heritage. Digital Applications in Archaeology and Cultural Heritage, 41. https://doi.org/10.1016/j.daach.2026.e00542

Deng, Y., & Gan, V. J. L. (2026). Motion-prior and Confidence-aware Gaussian Splatting (MCGS) SLAM for 3D scene reconstruction of indoor built environments. Advanced Engineering Informatics. https://www.sciencedirect.com/science/article/pii/S1474034626000091

Do, T. L. P., Choi, J., Le, V. Q., Gentet, P., Hwang, L., & Lee, S. (2024). HoloGaussian digital twin: Reconstructing 3D scenes with gaussian splatting for tabletop hologram visualization of real environments. Remote Sensing, 16(23), 4591. https://www.mdpi.com/2072-4292/16/23/4591

Du, H., Wang, H., Pan, Z., & Jiao, Y. (2025). A MomentumGS Based Large-Scale 3D Reconstruction Algorithm for Bridge Piers Using a Climbing Robotic Platform. 2025 12th International Forum on Electrical Engineering and Automation, IFEEA 2025, 31–35. https://doi.org/10.1109/IFEEA66847.2025.11388282

Du, H., Wang, H., Pan, Z., Jiao, Y., Zhang, X., & Gao, R. (2026). Three-Dimensional Reconstruction Algorithm for Concrete Bridge Piers Based on Octree-GS and the Climbing Robot Platform. Journal of Computing in Civil Engineering, 40(4). https://doi.org/10.1061/JCCEE5.CPENG-7052

Duan, D., Wang, Z., Xin, Y., & Ding, Y. (2025). Defect segmentation and 3D reconstruction in concrete structures using SAM 2 and 3D Gaussian splatting. Journal of Civil Structural Health Monitoring, 15, 3345–3360. https://doi.org/10.1007/s13349-025-00993-z

ElQasaby, A. R., Alqahtani, F. K., & Alheyf, M. (2022). State of the art of BIM integration with sensing technologies in construction progress monitoring. Sensors, 22(9). https://doi.org/10.3390/s22093497

Endalamaw, E. T., Mitra, R., & Mehrabian, M. (2026). SplatGauge: RGB-Only 3D Crack and Surface Change Metrology with Gaussian Splatting, GeoTransformer-ICP Registration, and M3C2-EP. 2026 IEEE 16th Annual Computing and Communication Workshop and Conference (CCWC), 1084–1091. https://doi.org/10.1109/CCWC67433.2026.11393714

European Commission. (2018). Guidelines for the waste audits before demolition and renovation works of buildings. https://ec.europa.eu/docsroom/documents/31521/

Fadilah, W. A., Murtiyoso, A., Landes, T., & Grussenmeyer, P. (2026). Metric assessment of 3D Gaussian Splatting for UAV-based urban heritage reconstruction. International Archives of the Photogrammetry, Remote Sensing and Spatial Information Sciences, XLVIII-2/W12-2026, 143–150. https://doi.org/10.5194/isprs-archives-XLVIII-2-W12-2026-143-2026

Furukawa, Y., & Ponce, J. (2010). Accurate, dense, and robust multiview stereopsis. IEEE Transactions on Pattern Analysis and Machine Intelligence, 32(8), 1362–1376. https://doi.org/10.1109/TPAMI.2009.161

Gao, K., Lu, D., He, H., Li, L., Xu, L., Chapman, M. A., & Li, J. (2025). Gaussian Building Mesh (GBM): Extract a building's 3D mesh with Google Earth and Gaussian splatting. Remote Sensing Applications: Society and Environment, 40, 101807. https://doi.org/10.1016/j.rsase.2025.101807

Gao, K., Lu, D., Li, L., Chen, N., He, H., Xu, L., & Li, J. (2025). Digital buildings analysis: 3D modeling, GIS integration, and visual descriptions using Gaussian splatting, ChatGPT/DeepSeek, and Google Maps Platform. IEEE Geoscience and Remote Sensing Letters, 22. https://ieeexplore.ieee.org/abstract/document/11151593/

Ghansah, F. A. (2024). Digital twins for smart building at the facility management stage: A systematic review of enablers, applications and challenges. Smart and Sustainable Built Environment, 14(4), 1194–1229. https://doi.org/10.1108/SASBE-10-2023-0298

Gordon, M., Zimmerman, L. von, Haradhun, O., Campanella, D., Bräutigam, M., & De Wolf, C. (2024). Digitising Building Materials for Reuse with Reality Capture and Scan-to-BIM Technologies. In C. Wolf, S. Çetin, & N. Bocken (Eds.), A Circular Built Environment in the Digital Age (1st ed. 2024, pp. 41–44). Springer International Publishing; Imprint Springer. https://doi.org/10.1007/978-3-031-39675-5_3

Grogan, J., Sattineni, A., & Kim, J. (2022). State of advances in reality capture for construction progress monitoring and documentation. In T. Linner, B. GarcÃ-a de Soto, R. Hu, I. Brilakis, T. Bock, W. Pan, A. Carbonari, D. Castro, H. Mesa, C. Feng, M. Fischer, C. Brosque, V. Gonzalez, D. Hall, M. S. Ng, V. Kamat, C.-J. Liang, Z. Lafhaj, W. Pan, … Z. Zhu (Eds.), Proceedings of the 39th international symposium on

automation and robotics in construction (pp. 614–621). International Association for Automation; Robotics in Construction (IAARC). https://doi.org/10.22260/ISARC2022/0086

Gumowski, S. (2025). Versteckte Werte im Bestand : Das UmBauLabor, ein Projekt von Baukultur Nordrhein-Westfalen. Pnd - Rethinking Planning 2025(1), 72-85, 72–85. https://doi.org/10.18154/RWTH-2025-03385

Hagedorn, P., Herbers, P., Waldow, K., Fuhrmann, A., & Bartels, N. (2026). Comparing 3D Gaussian Splatting and Laser Scanning for Assessing the Condition of Structural Concrete Elements for Circular Reuse. In F. Rahimian, M. R. Hosseini, A. Akanmu, Z. Lafhaj, & L. Ducoulombier (Eds.), Proceedings of the Conference on Smart and Sustainable Built Environment 2025, Lille, France (1st ed.). Springer. https://doi.org/10.1007/978-981-95-8489-5_53

Hakimi, O., Liu, H., & Abudayyeh, O. (2024). Digital twin-enabled smart facility management: A bibliometric review. Front. Eng. Manag., 11, 32–49. https://doi.org/10.1007/s42524-023-0254-4

Ham, Y., Michalkiewicz, M., & Balakrishnan, G. (2024). DRAGON: Drone and Ground Gaussian Splatting for 3D Building Reconstruction. 2024 IEEE INTERNATIONAL CONFERENCE ON COMPUTATIONAL PHOTOGRAPHY, ICCP 2024, IEEE International Conference on Computational Photography, 1–12. https://doi.org/10.1109/ICCP61108.2024.10644903

He, B., Chen, H., & Hu, Z. (2026). Region-Conscious Gaussian Splatting: Region-Aware Reconstruction for Outdoor Heritage Scenes. 2026 5th International Symposium on Computer Applications and Information Technology (ISCAIT), 114–117. https://doi.org/10.1109/ISCAIT69154.2026.11477180

Herbers, P., Von Rössing, L., & Markus, K. (2025). LiLoc - Defect Image Localization in Laser Scans. Proceedings of the 42nd International Symposium on Automation and Robotics in Construction (ISARC2025). https://doi.org/10.22260/ISARC2025/0198

Hou, J., Hou, R., & Bao, Y. (2025). Regularized three-dimensional Gaussians for large-scale building reconstruction with spatial prior. Engineering Applications of Artificial Intelligence. https://www.sciencedirect.com/science/article/pii/S0952197625014472

Hu, A., & Fukuda, T. (2025). Multi-Source Building Reconstruction: Integrating point cloud completion and image-based methods. Proceedings of the International Conference on Computer-Aided Architectural Design Research in Asia, 4, 265–274. https://doi.org/10.52842/conf.caadria.2025.4.265

Huang, B., Yu, Z., Chen, A., Geiger, A., & Gao, S. (2024). 2D Gaussian Splatting for geometrically accurate radiance fields. Proceedings of ACM SIGGRAPH 2024.

Huang, S., Jiang, N., Liang, H., Wu, R., & Li, H. (2025). Bridge Realistic Reconstruction Algorithm Based on Improved 3D Gaussian Splatting. Laser and Optoelectronics Progress, 62(16). https://doi.org/10.3788/LOP242428

Jamil, O., & Brennan, A. M. (2025). Immersive heritage through gaussian splatting: A new visual aesthetic for reality capture. Frontiers in Computer Science, 7, 1515609. https://doi.org/10.3389/fcomp.2025.1515609

Jia, Q., & He, J. (2026). High-fidelity 3D reconstruction of cultural heritage via super-resolution and progressive Gaussian splatting. NPJ HERITAGE SCIENCE, 14(1). https://doi.org/10.1038/s40494-026-02355-4

Jung, S., Lee, S., Choi, D., & Lee, S. (2025). Technology for 3D Recording of Cultural Heritage. In G. Marreiros, L. Grande, J. Llerena, L. Conceicao, H. Ko, M. Plaza, & M. Ricca (Eds.), DISTRIBUTED COMPUTING AND ARTIFICIAL INTELLIGENCE, SPECIAL SESSIONS II, 21ST INTERNATIONAL CONFERENCE (Vol. 1151, pp. 81–90). Universidad De Salamanca. https://doi.org/10.1007/978-3-031-80946-0_8

Kang, W., Ding, Y., Zhang, H., Deng, W., & Wu, J. (2025). The 3D Modeling Technology for Substation Surface Temperature Distribution Based on Thermal-Geometric Joint. 2025 IEEE 8th Advanced Information Technology, Electronic and Automation Control Conference (IAEAC), 8, 1–8. https://doi.org/10.1109/IAEAC65194.2025.11166397

Kerbl, B., Kopanas, G., Leimkühler, T., & Drettakis, G. (2023). 3D gaussian splatting for real-time radiance field rendering. ACM Transactions on Graphics, 42(4), 139:1–139:14. https://doi.org/10.1145/3592433

Kim, Y., Im, I., Park, S., Sohn, H., Park, S.-P., & Ha, T. (2026). Multi-Sensor Monitoring for Cultural Heritage Preservation: Overcoming Single-Modality Limits with RGB-IR Sensor Fusion. 2026 IEEE Conference on Virtual Reality and 3D User Interfaces Abstracts and Workshops (VRW), 1145–1146. https://doi.org/10.1109/VRW70859.2026.00247

Kobbelt, L., & Botsch, M. (2004). A survey of point-based techniques in computer graphics. Computers & Graphics, 28(6), 801–814. https://doi.org/10.1016/j.cag.2004.08.009

Koller, D., Turitzin, M., Levoy, M., Tarini, M., Croccia, G., Cignoni, P., & Scopigno, R. (2004). Protected interactive 3D graphics via remote rendering. ACM Transactions on Graphics, 23(3), 695–703. https://doi.org/10.1145/1015706.1015782

Krefft, L., & Hoegner, L. (2025). A method for crack detection and quantification in masonry using neural network-based image analysis. ISPRS Annals of the Photogrammetry, Remote Sensing and Spatial Information Sciences, X-4/W6-2025, 113–119. https://doi.org/10.5194/isprs-annals-X-4-W6-2025-113-2025

Lan, S., Liu, J., Zhang, M., & Jiang, J. (2025). A Low-Light Adaptive Framework for 3D Reconstruction of Indoor Cultural Heritage. 2025 International Conference on Culture-Oriented Science & Technology (CoST), 1–6. https://doi.org/10.1109/CoST68045.2025.00012

Levoy, M., Pulli, K., Curless, B., Rusinkiewicz, S., Koller, D., Pereira, L., Ginzton, M., Anderson, S., Davis, J., Ginsberg, J., Shade, J., & Fulk, D. (2000). The digital michelangelo project: 3D scanning of large statues. Proceedings of ACM SIGGRAPH 2000, 131–144.

Levoy, M., Stanford Computer Graphics Laboratory, & Galleria dell'Accademia, Florence. (1999). The digital Michelangelo project. http://graphics.stanford.edu/projects/mich/

Li, J., Wang, S., Yang, R., Shi, S., & Liu, Z. (2026). DLG-GS: Dynamic Lighting-Aware Real-Time 3D Gaussian Splatting for Weak-Texture Tunnel Scenes. Remote Sensing, 18(11), 1705. https://www.mdpi.com/2072-4292/18/11/1705

Li, X., Sheng, W., Tang, Y., Yu, Y., & Peng, Y. (2026). A UAV–3DGS–VR Workflow for Scenario-Comparable Immersive Review in Heritage Landscapes. Drones, 10(6), 404. https://www.mdpi.com/2504-446X/10/6/404

Li, Y., An, J., He, N., Li, Y., Han, Z., Chen, Z., & Qu, Y. (2025). A review of simultaneous localization and mapping algorithms based on lidar. World Electric Vehicle Journal, 16(2). https://doi.org/10.3390/wevj16020056

Li, Y., Ran, X., Xu, L., Lu, T., Yu, M., Wang, Z., Xiangli, Y., Lin, D., & Dai, B. (2025). Proc-Gs: Procedural Building Generation for City Assembly with 3D Gaussians. IEEE Computer Society Conference on Computer Vision and Pattern Recognition Workshops, 1997–2006. https://doi.org/10.1109/CVPRW67362.2025.00188

Liang, A., Wang, J., Pan, Y., Wang, H., Li, Y., &... (2026). Modeling Ancient Shu Road Relics of China Through Fisheye-Adaptive 3-D Gaussian Splatting Reconstruction Framework. IEEE Transactions on …. https://ieeexplore.ieee.org/abstract/document/11421779/

Liang, Y., Fang, Z., & Xu, Z. (2026). 3D Reconstruction and Building Energy Modeling for Existing Buildings via Image and Masked Gaussian Splatting. Journal of Building Engineering. https://www.sciencedirect.com/science/article/pii/S2352710226002391

Liang, Y., Xia, Y., Merzouk, M., & Xu, Z. (2026). From image to fire safety: An image-driven framework for as-is BIM reconstruction and fire risk assessment of existing buildings via semantic guidance. DEVELOPMENTS IN THE BUILT ENVIRONMENT, 25. https://doi.org/10.1016/j.dibe.2026.100869

Liang, Z., Chan, J. C. F., Zhang, J., Liang, Z., &... (2025). Optimized Language-Embedded 3DGS for Realistic Modeling and Information Storage of Historical Buildings. Proceedings of The …. https://easychair.org/publications/paper/fDS8/open

Liang, Z., Chan, J. C. F., Zhang, J., Liang, Z., Wang, B., Wang, M., & Cheng, J. C. P. (2026). Multimodal LLM-driven language-embedded 3D Gaussian splatting for semantic and realistic digitization of historical buildings. Automation in Construction, 181, 106628. https://doi.org/10.1016/j.autcon.2025.106628

CC BY

Liao, X., Liu, Y., Huang, Y., Luo, Y., Zhou, Z., & Chong, H. Y. (2026). Integrating CAD, BIM, immersive technology, and 3D Gaussian Splatting for construction model coordination with ISO 19650. Scientific Reports 16, 2410. https://www.nature.com/articles/s41598-025-32244-y

Liao, X., Zhou, B., Liu, Y., Zhang, L., Zhou, Z., &... (2026). Reconstruction of existing buildings for evacuation assessment under emergency situations using 3D Gaussian splatting and machine learning. Reliability Engineering & System Safety 267A, 111887. https://www.sciencedirect.com/science/article/pii/S0951832025010877

Liu, K., Sabek, M., Lee, G., Kinateder, M., & Gonzalez, V. A. (2025). Developing a Digital Twin-based Framework for Construction Fire Hazard Recognition Training. Proceedings of the International Symposium on Automation and Robotics in Construction, 1073–1080. https://doi.org/10.22260/ISARC2025/0139

Liu, W., Zhong, Y., Li, Y., Chen, X., Cui, J., Zhang, H., Xu, L., Lou, X., Shi, Y., Yu, J., & Zhang, Y. (2025). CityGo: Lightweight Urban Modeling and Rendering with Proxy Buildings and Residual Gaussians. Proceedings - SIGGRAPH Asia 2025 Conference Papers, SA 2025. https://doi.org/10.1145/3757377.3763866

Liu, X., Fan, W., Zhang, Y., Zhang, Z., Wan, Y., Yue, D., & Zhong, J. (2025). GS2Poly: Textured polygonal building reconstruction guided by Gaussian opacity fields. IEEE Transactions on Geoscience and Remote Sensing, 63, 1–17. https://doi.org/10.1109/TGRS.2025.3635414

Llull, C., Baloian, N., Bustos, B., Kupczik, K., Sipiran, I., & Baloian, A. (2023). Evaluation of 3D reconstruction for cultural heritage applications. 2023 IEEE/CVF International Conference on Computer Vision Workshops (ICCVW), 1634–1643. https://doi.org/10.1109/ICCVW60793.2023.00179

Luhmann, T., Robson, S., Kyle, S., & Boehm, J. (2019). Close-range photogrammetry and 3D imaging. De Gruyter. https://doi.org/10.1515/9783110607239

Luo, J., Yang, Z., Shi, P., & Ye, Q. (2026). Indoor scan-to-BIM automation: From mobile perception to 3D building modelling. Automation in Construction, 182, 106731. https://doi.org/10.1016/j.autcon.2025.106731

Ma, W., Tu, Q., Pan, J., Zhao, L., Tu, W., & Li, Q. (2024). 3D Gaussian radiation field modeling for real-scene bridges. Cehui Xuebao/Acta Geodaetica Et Cartographica Sinica, 53(9), 1694–1705. https://doi.org/10.11947/j.AGCS.2024.20240071

Maru, M. B., Lee, D., Tola, K. D., & Park, S. (2021). Comparison of depth camera and terrestrial laser scanner in monitoring structural deflections. Sensors, 21(1). https://doi.org/10.3390/s21010201

Mazzacca, G., Karami, A., Rigon, S., Farella, E. M., Trybala, P., & Remondino, F. (2023). NeRF for heritage 3D reconstruction. International Archives of the Photogrammetry, Remote Sensing and Spatial Information Sciences, XLVIII-M-2-2023, 1051–1058. https://doi.org/10.5194/isprs-archives-XLVIII-M-2-2023-1051-2023

Mildenhall, B., Srinivasan, P. P., Tancik, M., Barron, J. T., Ramamoorthi, R., & Ng, R. (2021). NeRF: Representing scenes as neural radiance fields for view synthesis. Commun. ACM, 65(1), 99–106. https://doi.org/10.1145/3503250

Mirocha, L. (2025). Beyond Digital Twins: 3D Gaussian Splatting, Game Engines and Crossmedia Cultural Heritage Representations. Proceedings of the Special Interest Group on Computer Graphics and Interactive Techniques Conference Talks, SIGGRAPH Talks '25. https://doi.org/10.1145/3721239.3734094

Montas-Laracuente, N., Delgado Martos, E., Pesqueira-Calvo, C., Intra Sidola, G., Maitín, A., Nogales, A., & García-Tejedor, Á. J. (2025). Automatic 3D reconstruction: Mesh extraction based on Gaussian splatting from Romanesque–Mudéjar churches. Applied Sciences, 15(15), 8379. https://doi.org/10.3390/app15158379

Morais, D., Suim Chagas, F., Baldivieso, T., Dias, G., & Rosa, P. (2024). Multi-Drone 3D Reconstruction of Architectural and Structural Entities. 2024 Brazilian Symposium on Robotics (SBR) and 2024 Workshop on Robotics in Education (WRE), 180–185. https://doi.org/10.1109/SBR/WRE63066.2024.10837817

Murtiyoso, A., & MacHer, H. (2025). Gaussian Splatting for Facade Orthophoto Generation - Comparison with MVS and TLS. International Archives of the Photogrammetry, Remote Sensing and Spatial Information Sciences - ISPRS Archives, 48, 1059–1064. https://doi.org/10.5194/isprs-archives-XLVIII-M-9-2025-1059-2025

CC BY

Mutlib, N. K., Baharom, S. B., El-Shafie, A., & Nuawi, M. Z. (2016). Ultrasonic health monitoring in structural engineering: Buildings and bridges. Structural Control and Health Monitoring, 23(3), 409–422. https://doi.org/10.1002/stc.1800

Nex, F., & Remondino, F. (2014). UAV for 3D mapping applications: A review. Applied Geomatics, 6(1), 1–15. https://doi.org/10.1007/s12518-013-0120-x

Nikolaidis, P., Zavoleas, Y., & Poulis, A. (2025). Real-time Monitoring of Ciltural Heritage Building in Greece through their Digital Twins: Visualization of adaptive reuse plans in xr collaborative environments. Proceedings of the International Conference on Education and Research in Computer Aided Architectural Design in Europe, 1, 389–398. https://www.scopus.com/pages/publications/105026189451?origin=resultslist

Nikolaidis, P., Zavoleas, Y., & Poulis, A. (2026). Application of a Digital Twin HBIM in the Context of Architectural Preventive Conservation and Adaptive Reuse Approaches of Heritage Monuments, with the Use of Extended Reality Technologies. Communications in Computer and Information Science, 2838 CCIS, 93–105. https://doi.org/10.1007/978-3-032-15069-1_8

Oh, J., & Yu, J. (2025). USD-based 3D archiving framework for time-series digital documentation of natural heritage. The International Archives of the Photogrammetry, Remote Sensing and Spatial Information Sciences, XLVIII-M-9-2025, 1097–1104. https://doi.org/10.5194/isprs-archives-XLVIII-M-9-2025-1097-2025

Oytun, M., & Atasoy, G. (2022). Effect of terrestrial laser scanning (TLS) parameters on the accuracy of crack measurement in building materials. Automation in Construction, 144, 104590. https://doi.org/10.1016/j.autcon.2022.104590

Page, M. J., McKenzie, J. E., Bossuyt, P. M., et al. (2021). The PRISMA 2020 statement: An updated guideline for reporting systematic reviews. BMJ, 372, n71. https://doi.org/10.1136/bmj.n71

Pan, Y., Braun, A., Brilakis, I., & Borrmann, A. (2022). Enriching geometric digital twins of buildings with small objects by fusing laser scanning and AI-based image recognition. Automation in Construction, 140, 104375. https://doi.org/10.1016/j.autcon.2022.104375

Pan, Y., Dong, M., Zhang, W., Xiang, H., Ma, Q., Li, Y., Huang, X., Zhou, H., Wang, Q., & Niu, W. (2025). 3D Digital Conservation of the Changsha Kiln Site and Its Ancient Ceramics. TRANSACTIONS IN GIS, 29(8). https://doi.org/10.1111/tgis.70173

Previtali, M., Barazzetti, L., & Roncoroni, F. (2026). Geometry reconstruction and orthophoto generation from 3D Gaussian Splatting in architectures with thin elements. International Archives of the Photogrammetry, Remote Sensing and Spatial Information Sciences - ISPRS Archives, 48, 383–390. https://doi.org/10.5194/isprs-archives-XLVIII-2-W12-2026-383-2026

Qin, J., Cheng, L., Qi, Z., Zhang, Z., & Liu, W. (2026). A 3D Gaussian Splatting-Based Framework for Occlusion-Aware Reconstruction of Immovable Cultural Heritage from Crowd-Sourced Data. Communications in Computer and Information Science, 2780 CCIS, 365–376. https://doi.org/10.1007/978-981-95-6730-0_26

Rábago, J., & Portuguez-Castro, M. (2023). Use of drone photogrammetry as an innovative, competency-based architecture teaching process. Drones, 7(3). https://doi.org/10.3390/drones7030187

Rašković, M., Ragossnig, A. M., Kondracki, K., & Ragossnig-Angst, M. (2020). Clean construction and demolition waste material cycles through optimised pre-demolition waste audit documentation: A review on building material assessment tools. Waste Management & Research, 38(9), 923–941. https://doi.org/10.1177/0734242X20936763

Rasshofer, R. H., & Geyer, K. (2005). Automotive radar and lidar systems for next generation ADAS. Advances in Radio Science, 3, 205–209. https://doi.org/10.5194/ars-3-205-2005

Remondino, F. (2011). Heritage recording and 3D modeling with photogrammetry and 3D scanning. Remote Sensing, 3(6), 1104–1138. https://doi.org/10.3390/rs3061104

Remondino, F., & El-Hakim, S. (2006). Image-based 3D modelling: A review. The Photogrammetric Record, 21(115), 269–291.

Remondino, F., Karami, A., Yan, Z., Mazzacca, G., Rigon, S., & Qin, R. (2023). A critical analysis of NeRF-based 3D reconstruction. Remote Sensing, 15(14), 3585. https://doi.org/10.3390/rs15143585

Rusinkiewicz, S., & Levoy, M. (2000). QSplat: A multiresolution point rendering system for large meshes. Proceedings of ACM SIGGRAPH 2000, 343–352. https://doi.org/10.1145/344779.344940

Rusinkiewicz, S., & Levoy, M. (2001). Streaming QSplat: A viewer for networked visualization of large, dense models. Proceedings of the 2001 Symposium on Interactive 3D Graphics, I3D '01, 63–68. https://doi.org/10.1145/364338.364350

Rüter, S., Waldow, K., Bartels, N., & Fuhrmann, A. (2025). 3D gaussian splatting for construction sites. In E. Noroozinejad Farsangi, A. H. Rasouli, N. Dawood, & G. Morrison (Eds.), Construction applications of virtual reality, volume 2 (pp. 37–52). Springer Nature Singapore.

Salah, R., Károlyfi, K. A., Szép, J., & Géczy, N. (2025). A structured framework for HBIM standardization: Integrating scan-to-BIM methodologies and heritage conservation standards. Digital Applications in Archaeology and Cultural Heritage, 37, e00420. https://doi.org/10.1016/j.daach.2025.e00420

Salman, A., & Ahmad, W. (2023). Implementation of augmented reality and mixed reality applications for smart facilities management: A systematic review. Smart and Sustainable Built Environment, 14(1), 254–275. https://doi.org/10.1108/SASBE-11-2022-0254

Sami Ur Rehman, M., Shafiq, M. T., & Ullah, F. (2022). Automated computer vision-based construction progress monitoring: A systematic review. Buildings, 12(7). https://doi.org/10.3390/buildings12071037

Santagati, C., Inzerillo, L., & Di Paola, F. (2013). Image-based modeling techniques for architectural heritage 3D digitalization: Limits and potentialities. International Archives of the Photogrammetry, Remote Sensing and Spatial Information Sciences, XL-5/W2, 555–560.

Schonberger, J. L., & Frahm, J.-M. (2016). Structure-from-motion revisited. Proceedings of the IEEE Conference on Computer Vision and Pattern Recognition (CVPR).

Schönberger, J. L., Zheng, E., Frahm, J.-M., & Pollefeys, M. (2016). Pixelwise view selection for unstructured multi-view stereo. In B. Leibe, J. Matas, N. Sebe, & M. Welling (Eds.), Computer vision – ECCV 2016 (pp. 501–518). Springer International Publishing.

Selman, Z., Musto, J., & Kobbelt, L. (2022). Scan2FEM: From point clouds to structured 3D models suitable for simulation. In F. Ponchio & R. Pintus (Eds.), Proceedings of the eurographics workshop on graphics and cultural heritage (GCH 2022). The Eurographics Association. https://doi.org/10.2312/gch.20221215

Sestras, P., Badea, G., Badea, A. C., Salagean, T., Roșca, S., Kader, S., & Remondino, F. (2025). Land surveying with UAV photogrammetry and LiDAR for optimal building planning. Automation in Construction, 173, 106092. https://doi.org/10.1016/j.autcon.2025.106092

Stefańska, A., Markowski, H., & Dixit, S. (2024). Three-dimensional laser scanning for structure documentation and construction management: A case study of renovation and rebuilt of metro tunnels. Ain Shams Engineering Journal, 15(5), 102665. https://doi.org/10.1016/j.asej.2024.102665

Stylianidis, E., Georgopoulos, A., & Remondino, F. (2016). Basics of image-based modelling techniques in cultural heritage 3D recording. In E. Stylianidis & F. Remondino (Eds.), 3D recording, documentation and management of cultural heritage (pp. 253–304). Whittles Publishing.

Suwardhi, D., Agustina, L. K., Andika, W., Widyastuti, R., Fadilah, W. A., Murtiyoso, A., & Remondino, F. (2026). Integrating terrestrial laser scanning and 3D Gaussian Splatting for heritage building documentation and monitoring. International Archives of the Photogrammetry, Remote Sensing and Spatial Information Sciences, XLVIII-2/W12-2026, 463–470. https://doi.org/10.5194/isprs-archives-XLVIII-2-W12-2026-463-2026

Waldschmidt, C., Hasch, J., & Menzel, W. (2021). Automotive radar — from first efforts to future systems. Proceedings of the IEEE, 109(2), 135–162. https://doi.org/10.1109/JPROC.2020.3010599

Wang, R., Hua, C., Shingys, T., Niu, M., Yang, Q., Gao, L., Zheng, Y., Yang, J., & Wang, Q. (2025). Enhancement of 3D Gaussian Splatting using Raw Mesh for Photorealistic Recreation of Architectures. 2025 15TH IEEE

CC BY

INTERNATIONAL CONFERENCE ON PATTERN RECOGNITION SYSTEMS, ICPRS, 1–9. https://doi.org/10.1109/ICPRS66293.2025.11302829

Wang, S., Nie, X., Narazaki, Y., Matiki, T., &... (2026). Three-dimensional Damage Visualization of Civil Structures via Gaussian Splatting-enabled Digital Twins. arXiv Preprint arXiv …. https://arxiv.org/abs/2602.16713

Wang, X., Lv, X., Shi, T., Bu, L., Bai, W., & Peng, K. (2025). The reconstruction method for static exterior model of digital twin railway station based on mobile vehicle. Scientific Reports, 15(1). https://doi.org/10.1038/s41598-025-96535-0

Wang, Y., Yang, X., Zhou, M., Qiu, K., & Wang, J. (2025). DirecGeo-GS: Direction-aware and geometry-enhanced Gaussian splatting for Tibetan temple symbols. JOURNAL OF SUPERCOMPUTING, 81(16). https://doi.org/10.1007/s11227-025-08046-4

Westoby, M. J., Brasington, J., Glasser, N. F., Hambrey, M. J., & Reynolds, J. M. (2012). "Structure-from-motion" photogrammetry: A novel, low-cost tool for geomorphology. Geomorphology, 179, 300–314. https://doi.org/10.1016/j.geomorph.2012.08.021

Wilson, A., Murtiyoso, A., Jenny, B., Darmawiguna, I. G. M., Suputra, P. H., Chandler, T., Kesiman, M. W. A., & Satriadi, K. A. (2025). 3D Gaussian Splatting for Archival of Balinese Temples from Community-Sourced Videos. 2025 IEEE International Conference on Imaging Systems and Techniques (IST), 1–6. https://doi.org/10.1109/IST66504.2025.11268436

Wu, C.-Y., Hsu, L.-S., & Hsu, C.-H. (2025). FlyGS: Online 3DGS Model Construction Using a MAVLink-Connected Drone. Proceedings of the 3rd International Workshop on UAVs in Multimedia: Capturing the World from a New Perspective, UAVM '25, 68–72. https://doi.org/10.1145/3728482.3757385

Wu, X., Liu, Y., Li, M., Guo, H., & Gou, Y. (2026). LiDAR-Guided 3D Gaussian Splatting with Differentiable UDF-Based Regularization for Mine Tunnel Reconstruction. Remote Sensing, 18(9). https://doi.org/10.3390/rs18091386

Wysocki, O., Schwab, B., Biswanath, M. K., Greza, M., Zhang, Q., Zhu, J., Froech, T., Heeramaglore, M., Hijazi, I., Kanna, K., Pechinger, M., Chen, Z., Sun, Y., Segura, A. R., Xu, Z., AbdelGafar, O., Mehranfar, M., Yeshwanth, C., Liu, Y.-C., … Jutzi, B. (2026). TUM2TWIN: Introducing the large-scale multimodal urban digital twin benchmark dataset. ISPRS JOURNAL OF PHOTOGRAMMETRY AND REMOTE SENSING, 232, 810–830. https://doi.org/10.1016/j.isprsjprs.2025.12.013

Xing, Y., Yang, S., Fahy, C., Harwood, T., & Shell, J. (2025). Capturing the past, shaping the future: A scoping review of photogrammetry in cultural building heritage. Electronics, 14(18). https://doi.org/10.3390/electronics14183666

Xiong, Z., Gordon, M., Byers, B., & De Wolf, C. (2022). Reality capture and site-scanning techniques for material reuse planning. Proceedings of IASS Annual Symposia, IASS/APCS 2022 Beijing Symposium: Sustainable Heritage Challenges and Strategies in the Preservation and Conservation of 20th Century Historic Concrete Shells. https://doi.org/10.3929/ETHZ-B-000580345

Xiong, Z., Li, X., Zhu, H., Tan, Y., & Li, J. (2026). LCSR: Low-cost surface reconstruction for outdoor monolithic buildings based on Gaussian splatting. Displays. https://www.sciencedirect.com/science/article/pii/S0141938226001411

Xu, H., Ma, L., Guan, H., & Li, J. (2025). Large-Scale Urban Scene Reconstruction Using 3D Gaussian Splatting and Satellite Imagery. IGARSS 2025-2025 IEEE …. https://ieeexplore.ieee.org/abstract/document/11242741/

Xu, X., Ran, B., Jiang, N., Xu, L., Huan, P., Zhang, X., & Li, Z. (2024). A systematic review of ultrasonic techniques for defects detection in construction and building materials. Measurement, 226, 114181. https://doi.org/10.1016/j.measurement.2024.114181

Xue, J., Hou, X., & Zeng, Y. (2021). Review of image-based 3D reconstruction of building for automated construction progress monitoring. Applied Sciences, 11(17). https://doi.org/10.3390/app11177840

Yan, Z., Mazzacca, G., Rigon, S., Farella, E. M., Trybala, P., & Remondino, F. (2023). NeRFBK: A holistic dataset for benchmarking NeRF-based 3D reconstruction. International Archives of the Photogrammetry, Remote

Sensing and Spatial Information Sciences, XLVIII-1/W3-2023, 219–226. https://doi.org/10.5194/isprs-archives-XLVIII-1-W3-2023-219-2023

Yu, R., Li, P., Shan, J., & Zhu, H. (2022). Structural state estimation of earthquake-damaged building structures by using UAV photogrammetry and point cloud segmentation. Measurement, 202, 111858. https://doi.org/10.1016/j.measurement.2022.111858

Yu, Y., Verbree, E., van Oosterom, P., Pottgiesser, U., Peng, Y., & Poux, F. (2025). From comparison to integration: A workflow evaluation of 3D Gaussian splatting and LiDAR point cloud for modern architectural heritage. Automation in Construction, 180, 106509. https://doi.org/10.1016/j.autcon.2025.106509

Yu, Y., Wang, Z., van Oosterom, P., Pottgiesser, U., Verbree, E., & Peng, Y. (2026). Reframing the "h" in HBIM: From systematic review to UML-based conceptual modeling. Frontiers of Architectural Research. https://doi.org/10.1016/j.foar.2026.02.007

Zahs, V., Anders, K., Kohns, J., Stark, A., & Höfle, B. (2023). Classification of structural building damage grades from multi-temporal photogrammetric point clouds using a machine learning model trained on virtual laser scanning data. International Journal of Applied Earth Observation and Geoinformation, 122, 103406. https://doi.org/10.1016/j.jag.2023.103406

Zhang, J., Fu Chan, J. C., Kwok, H. H. L., & Cheng, J. C. P. (2025). Adaptive and Automatic Illuminance Control of Semi-Open Historic Underground Sites Using Smart Glass Based on Digital Twins and 3D Reconstruction. ICCREM 2024: ESG Development in the Construction Industry - Proceedings of the International Conference on Construction and Real Estate Management 2024, 786–794. https://doi.org/10.1061/9780784485910.076

Zhang, Q., Wysocki, O., & Jutzi, B. (2025). GS4Buildings: Prior-guided gaussian splatting for 3D building reconstruction. ISPRS Annals of the Photogrammetry, Remote Sensing and Spatial Information Sciences, 10, 249–256. https://doi.org/10.5194/isprs-Annals-X-4-W6-2025-249-2025

Zheng, D., Liu, Y., & Jebelli, H. (2025). Towards Safer Construction Sites: A Preliminary Study on a Vision-Based Cyber-Physical System for Automated Hazard Detection. In A. Jafari & Y. Zhu (Eds.), COMPUTING IN CIVIL ENGINEERING 2025: COMPUTATIONAL AND INTELLIGENT TECHNOLOGIES (pp. 468–477).

Zheng, X., Zhang, S., Lin, W., Zhang, A., Mayol-Cuevas, W. W., Liu, Y., & Shen, J. (2025). CULTURE3D: A Large-Scale and Diverse Dataset of Cultural Landmarks and Terrains for Gaussian-Based Scene Rendering. 2025 IEEE/CVF International Conference on Computer Vision (ICCV), 29064–29074. https://doi.org/10.1109/ICCV51701.2025.02699

Zhou, L., Wu, G., Zuo, Y., Chen, X., & Hu, H. (2024). A comprehensive review of vision-based 3D reconstruction methods. Sensors, 24(7), 2314. https://doi.org/10.3390/s24072314

Zhu, J., & Wu, P. (2022). BIM/GIS data integration from the perspective of information flow. Automation in Construction, 136, 104166. https://doi.org/10.1016/j.autcon.2022.104166

Zhu, L., Shan, M., & Xu, Z. (2019). Critical review of building handover-related research in construction and facility management journals. Engineering, Construction and Architectural Management, 28(1), 154–173. https://doi.org/10.1108/ECAM-10-2018-0442

Zwicker, M., Pfister, H., Baar, J. van, & Gross, M. (2001). Surface splatting. Proceedings of ACM SIGGRAPH 2001, 371–378.

Zwicker, M., Pfister, H., Baar, J. van, & Gross, M. (2002). EWA splatting. IEEE Transactions on Visualization and Computer Graphics, 8(3), 223–238. https://doi.org/10.1109/TVCG.2002.1021576

CC BY

APPENDIX

Table 8: Database-specific search strings, searched fields, filters, and records retrieved.

Database	Interface / platform	Search field(s)	Verbatim search string	Filters applied	Records retrieved
Scopus	Elsevier Scopus, Advanced Search	TITLE-ABS-KEY (title, abstract, author keywords, indexed keywords)	`TITLE-ABS-KEY (("Gaussian Splatting" OR "Gaussian Splat*" OR "3D Gaussian*" OR "3DGS") AND ("construction" OR "building*" OR "infrastructure" OR "BIM" OR "AEC" OR "civil engineering" OR "built environment" OR "as-built" OR "scan-to-BIM" OR "reality capture" OR "progress monitoring" OR "site monitoring" OR "structural inspection" OR "defect detection" OR "facility management" OR "heritage"))`	Years: 2024 – now language: en	2,929
Web of Science	Clarivate Web of Science Core Collection, Advanced Search	TS = Topic (title, abstract, author keywords, Keywords Plus)	`TS=(("Gaussian Splatting" OR "Gaussian Splat*" OR "3D Gaussian*" OR "3DGS") AND ("construction" OR "building*" OR "infrastructure" OR "BIM" OR "AEC" OR "civil engineering" OR "built environment" OR "as-built" OR "scan-to-BIM" OR "reality capture" OR "progress monitoring" OR "site monitoring" OR "structural inspection" OR "defect detection" OR "facility management" OR "heritage"))`	Years: 2024 – now language: en	343
IEEE Xplore	IEEE Xplore, Command Search	"All Metadata" (title, abstract, index terms, author keywords)	`("All Metadata":"Gaussian Splatting" OR "All Metadata":"Gaussian Splat*" OR "All Metadata":"3D Gaussian*" OR "All Metadata":"3DGS") AND ("All Metadata":"construction" OR "All Metadata":"building*" OR "All Metadata":"infrastructure" OR "All Metadata":"BIM" OR "All Metadata":"AEC" OR "All Metadata":"civil engineering" OR "All Metadata":"built environment" OR "All Metadata":"as-built" OR "All Metadata":"scan-to-BIM" OR "All Metadata":"reality capture" OR "All Metadata":"progress monitoring" OR "All Metadata":"site monitoring" OR "All Metadata":"structural inspection" OR "All Metadata":"defect detection" OR "All Metadata":"facility management" OR "All Metadata":"heritage")`	Years: 2024 – now language: en	218
ACM Digital Library	ACM DL, Advanced Search (ACM Full-Text Collection)	All metadata fields ("Anywhere")	`[[All: "gaussian splatting"] OR [All: "gaussian splat*"] OR [All: "3d gaussian*"] OR [All: "3dgs"]] AND [[All: "construction"] OR [All: "building*"] OR [All: "infrastructure"] OR [All: "bim"] OR [All: "aec"] OR [All: "civil engineering"] OR [All: "built environment"] OR [All: "as-built"] OR [All: "scan-to-bim"] OR [All: "reality capture"] OR [All: "progress monitoring"] OR [All: "site monitoring"] OR [All: "structural inspection"] OR [All: "defect detection"] OR [All: "facility management"] OR [All: "heritage"]]`	Years: 2024 – now language: en	738
Google Scholar	Publish or Perish v8 (Harzing, 2007), Google Scholar query mode	Full-text and metadata (field-level restriction not supported)	`"Gaussian Splatting" OR "3D Gaussian Splatting" OR "3DGS" construction OR building OR infrastructure OR BIM OR "civil engineering" OR "built environment" OR "reality capture" OR heritage`	Result set capped at the first 1,000 records ranked by relevance (platform limit); truncation operators and nested Boolean logic are not supported, so the query was simplified accordingly	995
Total					**5,223**

CC BY

All searches were executed on 1 June 2026. The conceptual query combined a technology block with an AECO application block and was translated into the syntax of each platform; differences in field codes, wildcard handling, and Boolean nesting are reflected in the strings above. Records were exported in BibTeX format and deduplicated in Zotero by DOI and, where no DOI was available, by an exact match of title, first author, and publication year. Deduplication removed 897 records, leaving 4,326 unique records for screening.

CC BY